nature ecology & evolution

Article

https://doi.org/10.1038/s41559-023-01993-2

Minke whale feeding rate limitations suggest constraints on the minimum body size for engulfment filtration feeding

Received: 14 March 2022

Accepted: 5 January 2023

Published online: 13 March 2023

Check for updates

David E. Cade[1,2] ✉, Shirel R. Kahane-Rapport[2], William T. Gough[2], K. C. Bierlich[3,4], Jacob M. J. Linsky[1,5], John Calambokidis[6], David W. Johnston[3], Jeremy A. Goldbogen[2] & Ari S. Friedlaender[1]

Bulk filter feeding has enabled gigantism throughout evolutionary history. The largest animals, extant rorqual whales, utilize intermittent engulfment filtration feeding (lunge feeding), which increases in efficiency with body size, enabling their gigantism. The smallest extant rorquals (7–10 m minke whales), however, still exhibit short-term foraging efficiencies several times greater than smaller non-filter-feeding cetaceans, raising the question of why smaller animals do not utilize this foraging modality. We collected 437 h of bio-logging data from 23 Antarctic minke whales (*Balaenoptera bonaerensis*) to test the relationship of feeding rates (λ_f) to body size. Here, we show that while ultra-high nighttime λ_f (mean ± s.d.: 165 ± 40 lunges h^{-1}; max: 236 lunges h^{-1}; mean depth: 28 ± 46 m) were indistinguishable from predictions from observations of larger species, daytime λ_f (mean depth: 72 ± 72 m) were only 25–40% of predicted rates. Both λ_f were near the maxima allowed by calculated biomechanical, physiological and environmental constraints, but these temporal constraints meant that maximum λ_f was below the expected λ_f for animals smaller than ~5 m—the length of weaned minke whales. Our findings suggest that minimum size for specific filter-feeding body plans may relate broadly to temporal restrictions on filtration rate and have implications for the evolution of filter feeding.

The largest extant and extinct animals are marine vertebrate filter feeders[1,2]. Filter-feeding whales, sharks, rays and bony fish all have similar evolutionary trajectories, with filter-feeding morphologies and large body size deriving from smaller-bodied ancestors that probably pursued single prey items[3–6]. The co-evolution of gigantism and filter feeding in multiple, independent lineages[7] suggests a common mechanism at the interface of ecology and physiology. Changes in ocean productivity leading to increased concentrations of small prey amplify the efficiency of filter feeding, creating a selective pressure towards the development of feeding modalities that can capture abundant aggregations of small prey by filtering large volumes of prey-laden water[8].

Filter feeding is not restricted to the world's largest organisms, however. Many smaller organisms, including sessile invertebrates[9] as well as small- and medium-bodied fish[10–13] and Mobulid rays[14], are also obligate filter feeders. However, within mobile lineages where filter feeding occupies the upper size range of the group, there are also smaller group members that subsist as particulate (single-prey) foragers. For instance, the large-bodied whale shark (*Rhincodon typus*)

[1]Institute of Marine Science, University of California, Santa Cruz, CA, USA. [2]Hopkins Marine Station, Stanford University, Pacific Grove, CA, USA. [3]Division of Marine Science and Conservation, Nicholas School of the Environment, Duke University, Beaufort, NC, USA. [4]Marine Mammal Institute, Hatfield Marine Science Center, Oregon State University, Newport, OR, USA. [5]School of Biological Sciences, University of Queensland, Brisbane, Queensland, Australia. [6]Cascadia Research Collective, Olympia, WA, USA. ✉e-mail: davecade@stanford.edu

is the only filter-feeding carpet shark (order Orectolobiformes), and stingrays and non-mobulid eagle rays that feed on single prey items like teleost fish[15] are much smaller than filter-feeding mobulid rays[16]. There are also many single-prey-feeding cetacean species, such as dolphins (Delphinidae) and porpoises (Phoenidae), which are much smaller predators than the smallest filter-feeding baleen whales (Mysticeti). These broad trends in body size and feeding mode suggest a lower size limit for each group at which filter feeding becomes less efficient than particulate feeding, and the attainment of a minimum body size may be a prerequisite to the evolution of filter feeding.

In modern oceans, filter feeding at the largest scale is exhibited by several mysticete species that employ racks of keratinized baleen plates in lieu of teeth to sieve small prey from open water or sediment[17]. These lineages are characterized by specialized filter-feeding modes: continuous ram filter feeding in bowhead and right whales (Balaenidae); suction feeding by grey whales (*Eschrichtius*); and intermittent engulfment filtration (lunge feeding) in rorqual whales (Balaenopteridae). Lunge feeding utilizes taxon-specific adaptations[18–23] to enable a raptorial style of feeding involving the sequential high-speed approach of prey, engulfment of a large volume of prey-laden water and filtration through racks of keratinized baleen that can be repeated multiple times during a breath-hold dive[24].

The smallest extant rorqual whales, *Balaenoptera acutorostrata* (common minke whale, CMW) and *B. bonaerensis* (Antarctic minke whale, AMW) are, at mean adult body length of 7.7 ± 0.2 m (mean ± s.d.)[25], much larger than ancestral mysticetes (4.9 ± 1.5 m)[26], but smaller than all other rorqual species, which, prior to industrial whaling, could reach adult sizes of up to 30 m[27,28]. The minimum size of mammals is generally constrained by their thermoregulatory capacity[29]; in the marine environment, large body sizes counteract the heat loss associated with an aquatic lifestyle, with no mammalian taxa weighing less than 10 kg, and a common body-size optimum around 500 kg across multiple lineages[30]. Yet, the smallest filter-feeding whales are several tons[31], much larger than the maximum body size predicted by energy surplus models[30,32]. It is hypothesized that this release from maximum size restriction is due to the high engulfment capacity and energetic efficiency of lunge feeding[33], but it is as yet unclear how the intermittent filter-feeding adaptations that enhance the efficiency of large body size are limited at the smallest scale—minke whales. On short (dive-by-dive) time scales, AMW have lower energetic efficiency than larger engulfment feeders[33], but still have an order of magnitude higher energetic efficiency than similarly sized odontocetes or much larger balaenids. Extending the allometric relationship of body size to per-dive efficiency suggests that a lunge filter feeder could theoretically be as small as 10 kg and demonstrate approximately the same foraging efficiency as the much larger filter-feeding balaenid whales. This paradox suggests that intake restrictions that operate on longer time scales may better characterize the lower size limits of energetic efficiency for cetacean filter feeding.

Consumption rates in rorquals are constrained biomechanically (for example, the engulfment volume and the time it takes to approach, engulf and filter water), physiologically (for example, the breath-hold capacity utilized to feed at depth) and environmentally (for example, prey type, density and distribution[34]; Extended Data Fig. 1), and large body size can minimize the effects of some of these constraints. Perhaps most importantly, the engulfment volume of a lunge-feeding event exhibits positive allometry with body mass, such that a 5 ton AMW and an 80 ton blue whale (*Balaenoptera musculus*) are estimated to engulf water volumes equivalent to 42% and 135%, respectively, of their body masses with every feeding attempt[35,36]. This positive allometry of engulfment volume allows for greater mass-specific consumption with body size on a per-dive basis, even when accounting for decreased lunge rates resulting from longer processing times[37]. The combination of increasing per-lunge consumption with the decreasing mass-specific metabolic rate that is demonstrated across vertebrate lineages[38–40] largely explains the energetic benefits of large body size in filter-feeding cetacean lineages[33].

Conversely, some physiological and environmental constraints on performance are size-invariant. For example, cellular size is the same for small- and large-bodied organisms, leading to potential constraints in molecule delivery systems[41], and temporal cycles of prey abundance are not influenced by predator size. For filter-feeding rorqual whales, seasonal blooms in prey availability lead to periods of feast and fasting[42–44], and influence the correspondence of gestation periods (~11 months) across all rorquals[45], while diel vertical migration of swarms of invertebrates means that diurnal prey swarms are typically deeper than at night[46], requiring longer transit times that do not scale with body size[47].

To investigate how these constraints limit the minimum size of rorqual whales, we investigated the foraging behaviour of AMW in the Andvord Bay fjord complex (64.8° S, 62.7° W) of the West Antarctic Peninsula in 2018 and 2019 using suction-cup-attached bio-logging tags. We measured the feeding rates of 23 AMW of known length to test how these compare with feeding rates predicted from allometric expectations (Box 1). Departures from the null hypothesis would indicate environmental or behavioural modifications, restrictions or enhancements that either facilitate or constrain engulfment filtration feeding at either end of the body-size spectrum. When a potential constraint on minimum size was indicated, we investigated its scaling within AMW to identify the largest influences on AMW foraging

BOX 1

Scaling of feeding rates with body size

AMW forage in the prey-rich waters around Antarctica, primarily on Antarctic krill (*Euphausia superba*)[93,94]. Intake rate (λ, measured in units of biomass or energy per time) for rorquals is a product of feeding rate (λ_f), mean prey density in the engulfed water mass (λ_ρ), and engulfment volume (EV). Probably due to the balance of energy consumed with energy expended, in multiple taxa λ has been found to scale with mass (M) to a power of approximately 0.75 (refs. [95–104]; Supplementary Box 1). For comparability, the whales in our study were limited to animals feeding on similar prey (krill) in a similar manner (lunge feeding). As a starting point for comparison, our null hypothesis assumes mean prey density in engulfed water does not scale with body length, hence:

$$\lambda = \lambda_f \times \mathrm{EV} \propto M^{0.75} \quad (1)$$

Given that EV per lunge scales across species[36] proportionally to body length (L)$^{3.57}$, and mass scales across species proportionally to $L^{2.64}$, we expect that, when comparing species:

$$\lambda_f = \alpha \frac{M^{0.75}}{\mathrm{EV}} = \alpha \frac{(L^{2.64})^{0.75}}{L^{3.57}},$$
$$\text{or equivalently} : \log(\lambda_f) = \log(\alpha) + -1.59 \times \log(L), \quad (2)$$

where α is an unknown intercept. Our null hypothesis is therefore that the slope of the interspecific line relating log body length to log feeding rate in AMW from our study compared with prior published data from blue whales (*Balaenoptera musculus*) and humpback whales (*Megaptera novaeangliae*) would be −1.59. For AMW, which have EV $\propto L^{3.16}$ and $M \propto L^{3.09}$ (ref. [36]), the intraspecific null hypothesis gives an expected slope of −0.84.

https://doi.org/10.1038/s41559-023-01993-2

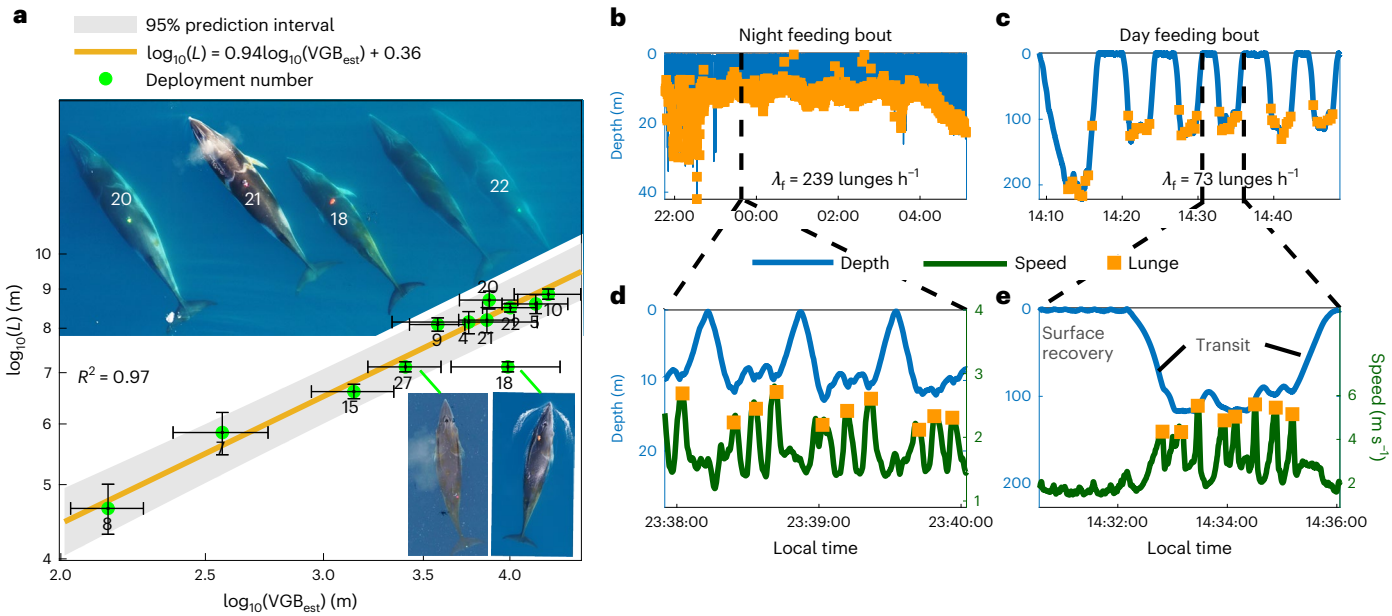

Fig. 1 | AMW size and feeding bouts examples. a, Relationship of estimated AMW ventral groove blubber (VGB) length (equivalent to buccal cavity length) to total length (L, measured via aerial photogrammetry) for the 12 deployments with both types of data. Buccal cavity length (VGB_{est}) is estimated from the mean calculated distance travelled during engulfment, integrating speed from mouth open to mouth closed as observed from on-animal cameras (Extended Data Table 1 and Supplementary Video 1), allowing an estimation of total body length for whales without aerial imagery (n for each data point listed in Extended Data Table 1). Horizontal error bars are standard error, vertical error bars are 95% highest posterior density centred around the mean (see Methods). Note log scale. Deployments 18 and 27 were on the same whale on different days. VGB_{est} for 18 appears to be biased by placement of the camera very close to the nares, so it was excluded from the regression. **b**, Depth profile and all lunges for the foraging bout with the highest feeding rate (λ_f) across all whales. **c**, Depth profile and all lunges for the daytime foraging bout with the highest λ_f from the same deployment (bb190226-56) as **b**. **d**,**e**, Depth and speed profiles for a portion of each feeding bout during nighttime (**d**) and daytime (**e**). Note that inter-lunge intervals are similar (10 lunges in 2 min at night versus 8 lunges in 2.5 min during the day), but feeding rates on deeper patches are limited by surface recovery and vertical transit time (see Extended Data Fig. 1). Aerial images courtesy of Duke Marine Robotics and Remote Sensing.

energetics. The temporal constraints we identify have implications for how the minimum size in other marine filter-feeding lineages may be similarly constrained by the energetic need to maximize the volume of prey-laden water that can be filtered in the time available for foraging.

Results

Body lengths were determined for 23 individuals (Extended Data Table 1) of the 27 total AMW tag deployments >1 h. Thirteen whales were directly measured using unoccupied aerial system (UAS) photogrammetry and ten lengths were estimated from regressing total length (L) on estimated buccal cavity length (VGB_{est}, derived from the distance travelled during engulfment; Fig. 1a). A total of 273 day hours and 133 night hours of tag data were analysed. Additionally, 17 krill-feeding humpback whales (237 day hours, 105 night hours) and 31 blue whales (319 day hours, 181 night hours) from previously published data[33,48,49] were utilized for comparison.

A total of 4,961 daytime lunges and 16,144 nighttime lunges were identified in 437 total hours (day hours + night hours + twilight hours) of AMW tag data. A total of 267 hours (61%) were identified as part of a foraging bout, of which 176 were during the day (64% of total daytime data) and 75 were at night (57% of total nighttime data), with 16 feeding hours during twilight periods. AMW feeding rates (minimum of 20-min bouts) ranged from 15 to 236 lunges h^{-1} (Fig. 1b), with a mean feeding rate during a foraging bout (weighted by bout duration, mean ± s.d.) of 85 ± 56 lunges h^{-1} (daytime only: 53 ± 10 lunges h^{-1}; nighttime only: 165 ± 40 lunges h^{-1}). For dives with multiple lunges, the mean inter-lunge interval (ILI) across deployments was 17.9 ± 9.2 s. The proportion of time spent feeding between day and night was similar, and there was not a relationship between the proportion of time spent feeding and body length (Extended Data Fig. 2), although sample size was limited to at most two days or nights of feeding for each whale. The most intense feeding occurred near the surface during the first half of the night (Fig. 2a). Mean depth of foraging dives during the day was 72 ± 72 m, and mean number of lunges per dive was 3.9 ± 2.9. At night, mean depth of foraging was 28 ± 46 m and mean number of lunges per dive was 3.4 ± 2.6.

Within AMW, feeding rate scaled with body size with a slope not significantly different from that predicted from allometry ($F_{(1,12)}$ = 0.006, P = 0.94; Fig. 2e). However, when limited to daytime feeding only, the slope was not significantly different from 0 ($F_{(1,19)}$ = 0.192, P = 0.67). The predominantly deep feeding during the day and shallow feeding at night (Fig. 2a) meant that partitioning data into deep feeding and shallow feeding gave similar results (Fig. 2f,g,i,j), with the shallow-feeding slope not significantly different from that predicted by allometry ($F_{(1,14)}$ = 0.203, P = 0.66), and the deep-feeding slope not significantly different from 0 ($F_{(1,16)}$ = 0.032, P = 0.86).

Across species, the feeding rate slope was significantly less steep than that predicted by allometry ($F_{(1,34)}$ = 33.4, P < 0.001; Fig. 2e,h and Extended Data Fig. 3), implying that small whales were feeding less per unit time than would be expected by allometry. However, nighttime ($F_{(1,44)}$ = 0.024, P = 0.87) and shallow ($F_{(1,51)}$ = 3.65, P = 0.06) feeding slopes were not significantly different from the predicted slopes, while daytime ($F_{(1,122)}$ = 177, P < 0.001) and deep ($F_{(1,120)}$ = 159, P < 0.001) feeding slopes were significantly less steep.

Biomechanical, physiological and environmental limits on λ_f

ILI on any given dive would be expected to scale with body size if the environment permitted the biomechanically maximum lunge rate—that

https://doi.org/10.1038/s41559-023-01993-2

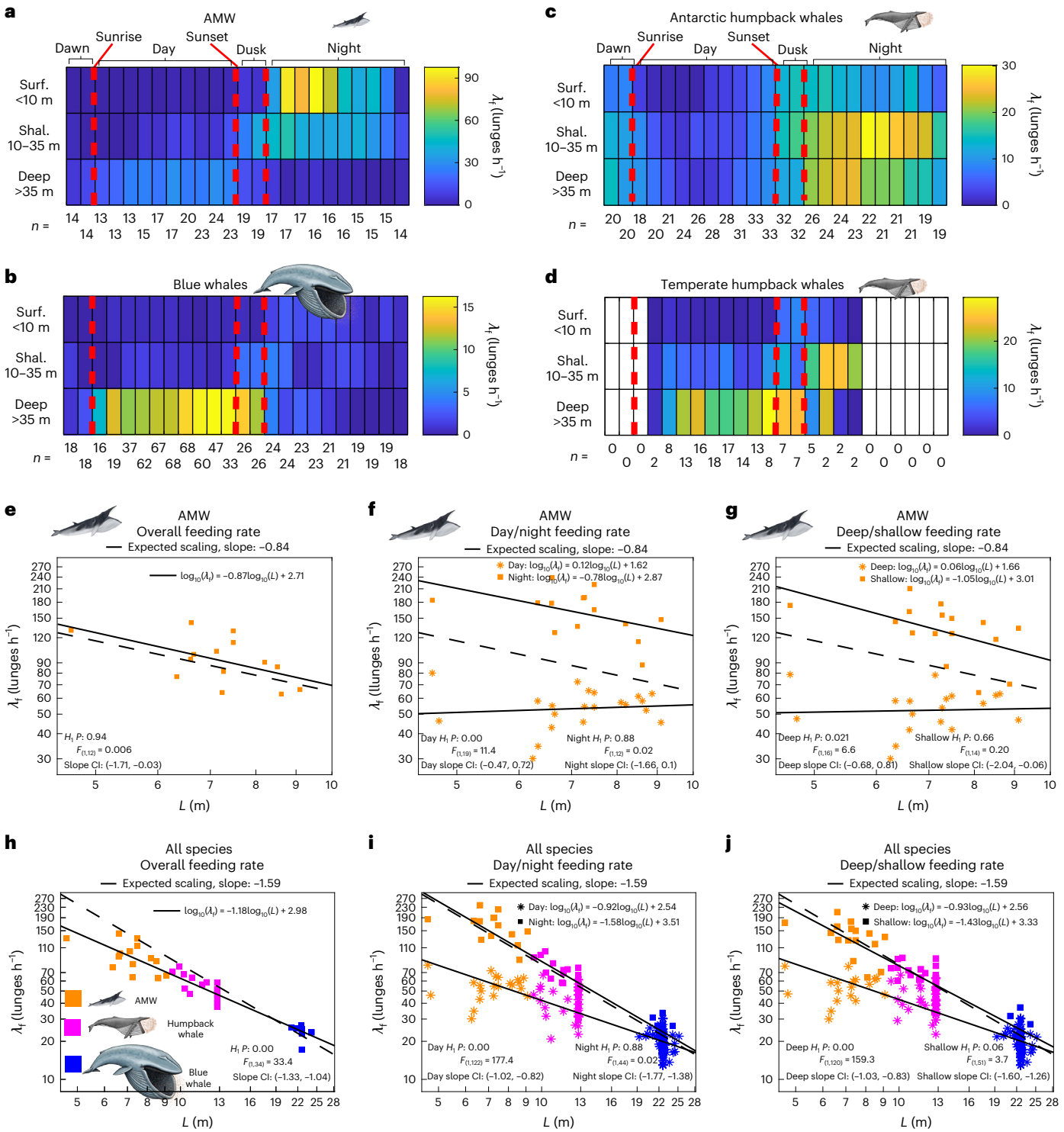

Fig. 2 | Feeding rates and scaling of feeding rates with body size. a–**d**, Feeding rates by depth and time for AMW (**a**), blue whales (**b**), Antarctic humpback whales (**c**) and terperate humpback whales (**d**). Surf., surface feeding; shal., shallow feeding. To account for differences in day length between deployments, day and night periods for each deployment were divided into ten periods of equal duration, and dusk and dawn were divided into two periods each (that is, the first day period is the feeding rate in the first tenth of the time that the sun is above the horizon). Rates were averaged across deployments by diel period. *n* = number of deployments with data for at least half the diel period (the threshold to be included) is listed below each period. All tags for krill-feeding humpback whales outside the Antarctic fell off before the first 40% of the night had passed. **e**–**j**, Regressions of feeding rates within foraging bouts against body length (*L*). Each point is the mean individual feeding rate (**e**,**h**), or the mean rate separated by day/night (**f**,**i**) or deep/shallow (35 m depth cut off; **g**,**j**). For overall feeding rates, animals were included if they fed at least 2 h in both day and night. In sub-categories (day/night or deep/shallow), animals were included if the deployment contained at least 2 h feeding in the indicated mode. Slope 95% confidence intervals (CI) and *F*-statistics are displayed, *P* values are for the two-sided *F*-test of the hypothesis (H_1) that the indicated regression has a slope different from the expected scaling slope. Both axes are log scales. Intercepts for expected scaling lines were arbitrarily chosen for visual display and are consistent across panels. Credits: minke whale (panels **a**,**e**–**h**), Audrey Nguyen; humpback whale and blue whale (panels **b**–**d**,**h**), Alex Boersma.

https://doi.org/10.1038/s41559-023-01993-2

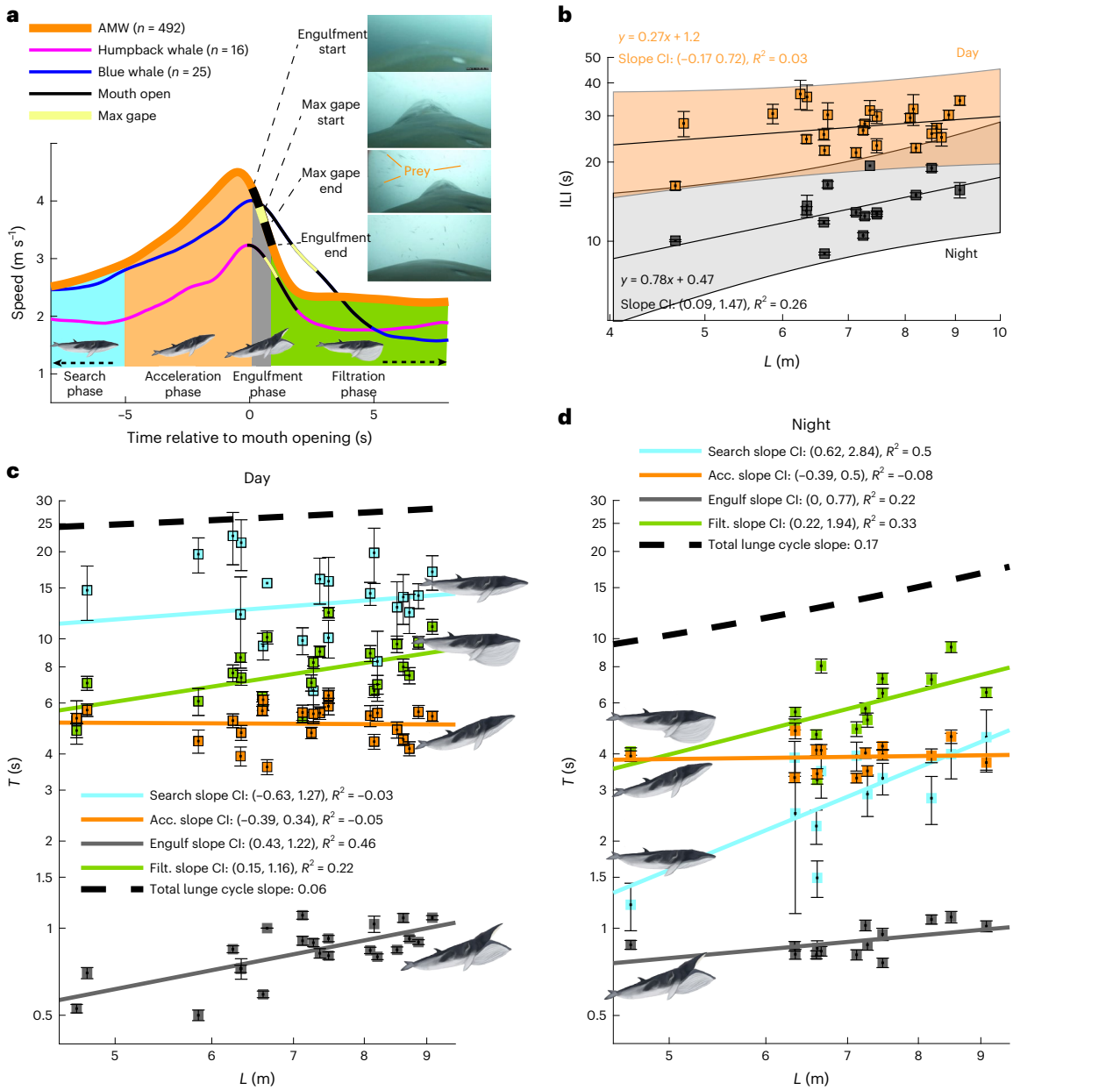

Fig. 3 | Phases of lunge feeding related to body length. a, Mean AMW lunge speed profile (derived from accelerometry data) and timing of engulfment (from video observations). *n* is number of lunges examined. Humpback and blue whale profiles shown for comparison, redrawn from ref. [81] with mean speed profiles from the expanded dataset of ref. [92]. Still images from Supplementary Video 1. **b**, Regressions of $\log_{10}$ mean inter-lunge interval (ILI) on dives deeper than 20 m during the day (shallower than 20 m at night) against $\log_{10}$ individual body length for AMW. ILI was calculated for all dives with at least two lunges. CI, 95% confidence interval; error bars, standard error; *n*, number of dives and reported in Extended Data Table 1. **c**,**d**, Relationships of log body length (*L*) of AMW to the log timing (*T*) of daytime (**c**) or nighttime (**d**) lunge phases (*n* = a subset of 30 lunges per whale, see Methods). **c**, Filtration and engulfment demonstrated significant relationships with body length. Total lunge cycle was the sum of filtration ($\log_{10}(T) = 0.66\log_{10}(L) + 0.32$) and engulfment ($\log_{10}(T) = 0.82\log_{10}(L) - 0.79$) regressions, and the mean acceleration (5.1 ± 1.6 s) and search (13.8 ± 4.7 s) times. **d**, At night, filtration, engulfment and search durations demonstrated significant relationships with body length. Engulfment timing at night was estimated from the speed profile, while daytime values were calculated from video observations. Total lunge cycle at night was the sum of filtration ($\log_{10}(T) = 1.1\log_{10}(L) - 0.15$), engulfment ($\log_{10}(T) = 0.38\log_{10}(L) - 0.37$) and search ($\log_{10}(T) = 1.7\log_{10}(L) - 1.0$) regressions, and the mean acceleration (3.9 ± 0.5 s) time. Two search values at night were excluded from the regression as outliers (standard error ≥ mean). Acc., acceleration; filt., filtration. Error bars are standard error. Slope CI is 95% confidence interval, displayed with adjusted R^2, axes are log scale. Credit: minke whale (panels **a**,**c** and **d**), Audrey Nguyen.

is, if ILI was only determined by approach and processing times[37]. We found no relationship between ILI and body length in AMW during deep daytime feeding, and a positive relationship during shallow nighttime feeding (Fig. 3b). The daytime relationship is largely driven by the distance between high-quality prey patches, implying that the environmental constraint of search/transit time between the end of one lunge cycle and the start of the next (Fig. 3c) will be largely size-invariant. In contrast, search time was only a small component of nighttime ILI (Fig. 3d), implying that patches with sufficient quality for feeding were closely distributed.

The component of ILI due to filtration, temporally the largest biomechanical constraint, demonstrated a positive relationship with

https://doi.org/10.1038/s41559-023-01993-2

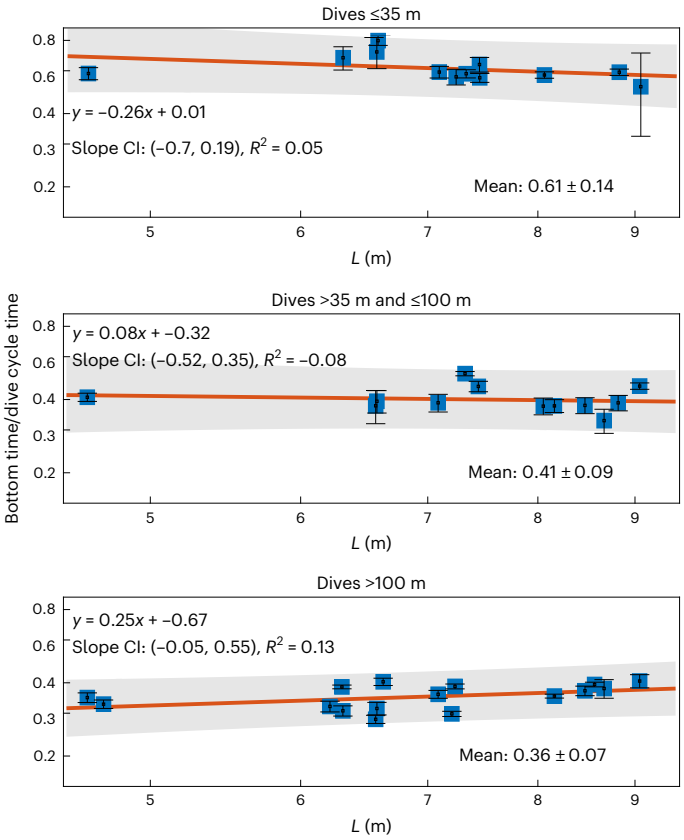

Fig. 4 | Relationship between body length and the mean proportion of available bottom time on an AMW daytime foraging dive with >2 lunges, binned by depth. Dive cycle length = dive time + the surface interval following the dive. Legends display the mean ± s.d. of all individuals combined. Error bars are standard error. Number of dives (*n*) for each data point listed in Extended Data Table 1, only animals with at least two dives in the depth category were included. CI are 95% confidence intervals.

body length (Fig. 3c,d), with a 9 m AMW filtering for ~50% longer than a 5 m AMW, while the relationship between body length and approach time (the time to accelerate from cruising speed to lunging speed) had a slope not significantly different from 0 (Fig. 3c,d). Engulfment time also scaled positively with body length, although the magnitude of variation was small compared with the overall lunge duration (Fig. 3c,d).

We found no relationship between mean dive depth or mean dive duration with AMW body length (Extended Data Fig. 4a,b). However, the amount of time AMW spent on a deep dive relative to dive depth increased with body size (Extended Data Fig. 4c). Similarly, the surface time on either side of a foraging dive (that is, oxygen loading time) increased with dive length (Extended Data Fig. 5). The relationship of bottom time available for foraging to overall dive cycle length decreased with depth and demonstrated a relationship with body length only for dives >100 m (Fig. 4).

Maximum feeding rates

The combination of physiological, biomechanical and environmental constraints determines the length of the ILI, which, in turn, limits the maximum feeding rate in each diel period (equation (3)). Nighttime feeding rates, dominated by near-surface lunges (Fig. 2a) that minimize the physiological constraint of feeding without access to oxygen, were therefore controlled mostly by the biomechanical constraints of filter time and approach time (Fig. 3d). While approach time and search time are largely size-invariant, filter time is strongly related to body size (Fig. 3c,d). Thus, as body size decreases, the proportion of ILI due to size-controlled parameters decreases (Extended Data Fig. 6), approaching an asymptote of size-invariant, environmentally controlled λ_f (Fig. 5). Maximum nighttime feeding rates scale with body length, with curvature that drops below the observed regression line near 5 m body length (Fig. 5). The slopes of daytime maximum feeding rates were also controlled by biomechanical constraints, but rates were lower overall due to both the increase in search time between lunges and the physiological necessity to recover oxygen debt at the surface between foraging dives. The physiological relationship of this bottom time ratio to body length (Fig. 4) has a large effect on the slope and curvature of the predicted maximum λ_f lines. If prey is deep, maximum λ_f declines rapidly with decreasing size (Fig. 5). The vertical movement of prey (shallower at sunset and deeper at sunrise) then results in an increasing night–day difference in λ_f as body size decreases. Consequently, the extreme seasonal variation in day length at high latitudes then implies a disparity in the abilities of small and large animals to meet required needs if prey is deep for extended periods during seasons with extended daylight (Supplementary Box 2).

Discussion

Explanations for why the largest animals are filter feeders often highlight how gigantism enables the efficient exploitation of large, dense, heterogeneously distributed patches of prey[33,50–52]. The flip side of this question is less often explored: what is the minimum body size at which a specific filter-feeding modality is still efficient? In a discussion on whale shark size, the largest extant fish species and an obligate filter feeder, the authors of ref. [1] approach this question from an evolutionary angle, asking, "Are animals able to become planktivores because they are so large, or do large sizes result from planktivory?". Rorqual whales, a group with species that span more than an order of magnitude in body mass yet feed on the same prey using the same feeding style, are a good study system for this question because their unique engulfment filtration-feeding style is energetically expensive[53–55], implying that energetic limitations to feeding efficiency should be apparent. Additionally, rorqual whales have an extensive fossil record of smaller-bodied ancestors that provides evidence of a transition from obligate particulate feeding to obligate filter feeding[26,56]. Extant rorqual whales are giant (adult sizes 8–30 m[27,28]) filter feeders that coexist in environments with much smaller whales that feed on single prey items (for example, the 1.5 m harbour porpoise), implying that there is no apparent thermoregulatory or physiological restriction on small body size.

The increasing efficiency of filter feeding with body size[33] supports the second part of the above question: once planktivory evolves, larger sizes increase efficiency. Here, we provide evidence in rorqual whales that the first part of the question also holds: that large size is required for successful filter feeding in this clade. The interplay between these two facets of how gigantism and filter feeding overlap has implications for how both strategies evolve and suggests a broader theme for all filter feeders that we refer to as the minimum-size constraint (MSC) hypothesis: while the maximum size of a filter-feeding body plan will be restricted by physical properties[57], the minimum size is restricted by the energetic efficiency of filter feeding and the time required to extract sufficient particles from the water.

An MSC would allow for two alternative strategies for juvenile forms of obligate filter-feeding species (Supplementary Box 3): (1) birth young at or above the minimum body size for suspension feeding; or (2) for some initial stage, young must adopt an alternative feeding strategy, which could include the mammalian strategy of dependence on lipid-rich maternal milk[58]. Length at weaning for minke whales, based on twentieth-century whaling data, is reportedly 4.5–5.5 m[43,59], although *B. bonaerensis* was not differentiated from *B. acutorostrata* until the 1990s[60], so further differentiation among species has not been possible. When we examined the scaling of maximum feeding rates

https://doi.org/10.1038/s41559-023-01993-2

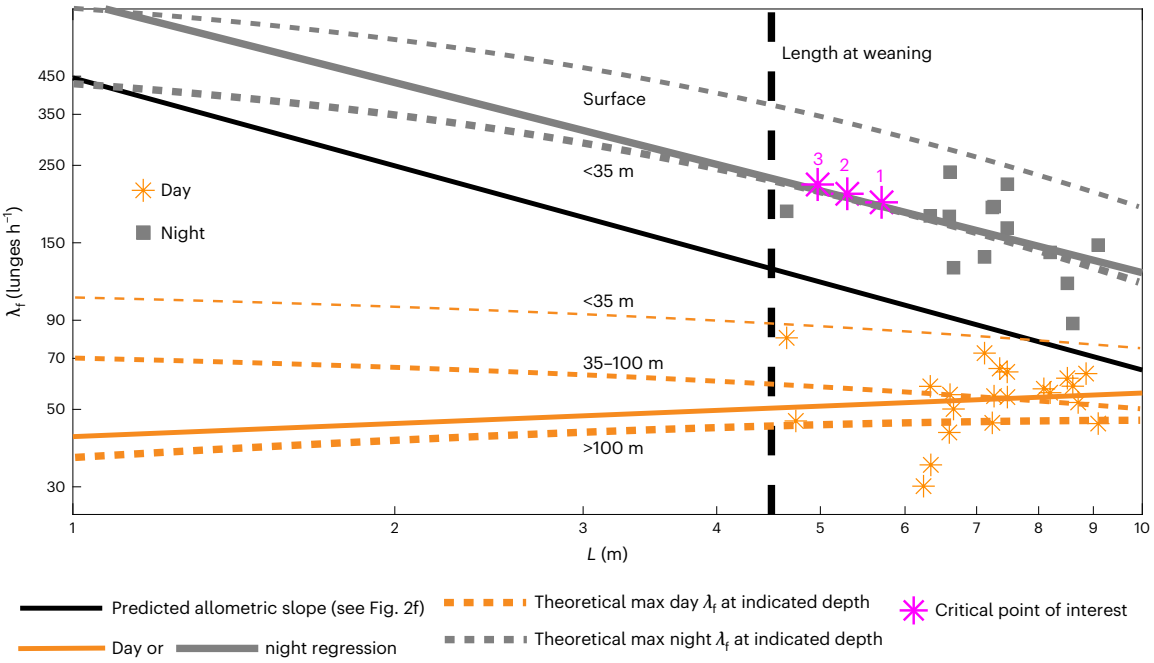

Fig. 5 | Predicted maximum possible feeding rates compared with observed rates for AMW. Both axes are log scales. Points and regression lines are the same as in Fig. 2f. Grey (night) and orange lines (day) are the predicted maximum possible feeding rate limited by observed biomechanical, physiological and environmental temporal constraints, equation (3)). Night 'surface' line utilizes a bottom time proportion of 100%, that is, no physiological constraint due to surface recovery or transit. Lower bound of reported length at weaning for AMW = 4.5 m[43]. Critical points of interest: (1) the body length at which the slope of (either) maximum night feeding line falls below the slope of the night regression line; (2) the length at which the slope of (either) maximum night feeding line changes concavity; and (3) the length at which the predicted maximum night feeding <35 m falls below the values predicted by regression.

(Fig. 5), we therefore expected to see evidence of an MSC on rorqual whale efficiency at body lengths of 4.5–5.5 m or smaller.

Across systems, animals seek to maximize their intake during periods of active foraging[61–63]. Here, we show that AMW feed at extremely high foraging rates, which are limited temporally by biomechanical, physiological and environmental constraints, and that these rates are near the maximum predicted by the regression of these constraints on body size (Fig. 5). Average feeding rates for this species are less than would be predicted from the feeding rates and engulfment capacities of larger species (Fig. 2h); however, shallow (typically nighttime) feeding rates are equivalent to those predicted from allometry, suggesting that these shallow feeding periods are a critical component of minke whale foraging strategy.

Two separate factors linked to time of day appear to interact to limit AMW energetic intake at small body size. First, overall intake is limited during the day as animals get smaller, when prey patches are deep, by the proportionally less bottom time per dive cycle available to smaller animals (Fig. 4). Second, during the day a greater proportion of each lunge cycle is composed of the size-invariant constraints of search and acceleration (Fig. 3c). These factors imply that smaller AMW are not able to increase their intake rate to meet their expected metabolic needs, so the only available recourse to increase their total intake would be to feed for greater proportions of the day (Extended Data Fig. 2) or the feeding season, both factors that eventually reach size-invariant maxima and that conflict with other life-history needs such as rest and reproduction.

At night, however, when prey is shallower, smaller whales increase their feeding rate coincident with allometric predictions (Fig. 2f,g). Shallow prey largely negates the breath-hold constraint and allows for rapid, near constant feeding (Figs. 2 and 3). However, as whales get smaller, the proportion of each lunge cycle taken up by size-invariant constraints increases (Extended Data Fig. 6), leading to nonlinear effects in the scaling of maximum possible feeding rates (Fig. 5) that constrain maximum feeding below the extension of the regression line. The slope of the nighttime predicted maximum feeding rate line is less than the slope of the regression line for $L < 5.76$ m, the slope of the nighttime maximum feeding line changes curvature from concave up to concave down for $L < 5.35$ m, and the predicted maximum feeding for shallow feeding <35 m falls below the value of the regression line for $L < 4.97$ m (Fig. 5). The combination of maximum possible feeding rates that are proportionally lower than expected during both day and night suggests an overall reduction in efficiency below the length of weaning—essentially, the scaling of the biomechanics of lunge feeding restricts the ability of small animals (<5 m) to filter enough water to meet their metabolic needs.

The apparent MSC on rorqual whales suggests an adjustment to the question discussed earlier by ref. [1], "How can giant filter-feeders arise if both gigantism and filter feeding are necessary preconditions for the other?" Engulfment filter feeding was thought to first arise in mysticetes the size of today's AMW, and evidence from baleen morphology suggests that intermittent engulfment filtration evolved prior to the continuous ram filtering of balaenids[56,64]. With few exceptions (for example, the 12.5 m *Norrisanima miocaena*[65]), it was not until the last ~5 million years that mysticetes evolved gigantic body sizes >10 m[26]. This increase in gigantism is thought to coincide with increased seasonal upwelling, the establishment of the Antarctic Circumpolar Current and larger diatom availability[66], encouraging the formation of predictable regions of giant prey patches at depth that are best exploited by giant body sizes. Ocean conditions when baleen first arose in mysticetes 30 million years ago (Ma) are less clear, but the quadrupling of filtration volume per time we observed for small-bodied whales in shallow waters suggests that oceans at this time may have had prey distributions similar to the waters around the West Antarctic Peninsula today, with reliably accessible, dense patches of surface prey that could be efficiently exploited at prehistoric body sizes (Supplementary Box 4).

In contemporary oceans, all rorqual whale species have the ability to lunge feed on krill, suggesting the question of what axis of heterogeneity has driven speciation in this clade[67]. As one facet of the answer, our results suggest that different body sizes appear to be best suited to capture different prey configurations. Smaller, more manoeuvrable animals[68,69] efficiently exploit small, scattered patches of surface krill, while larger organisms are better able to exploit deep, extensive and dense prey patches. All rorqual species except blue whales are thought to at least occasionally forage on additional types of swarming or schooling prey[70] using both lunge feeding and alternative techniques[71–74]. CMW, for instance, feed regularly on both krill and schooling fish[75,76], reducing the number of lunges required to meet energy demands. Lunge feeding on fish is thought to be enhanced by large body size, which may paradoxically delay the flight response in prey[77], yet there also appears to be an upper size limit at which lunge feeding on fish is no longer effective because long engulfment durations of blue-whale-sized animals allow time for prey to escape[77].

To overcome the MSC and the inefficiencies of filter feeding before the development of gigantic body sizes, early edentulous mysticetes, with adult sizes generally around 4–5 m in length or smaller[26], probably fed primarily on prey with higher energy yields or greater availability than the vertically migrating planktonic krill supply of extant AMW; that is, they were probably fish feeders that transitioned to filter feeding when ocean conditions encouraged the formation of dense, stable, relatively shallow patches of invertebrates. The MSC for rorquals we have presented here is consistent with the fossil record, which suggests that baleen first evolved 30 Ma in small whales and probably enabled filter feeding to supplement particulate feeding[78]. Subsequently, the biomechanical structures that enabled raptorial, bulk feeding on small, high-energy schooling prey like fish arose coincident with larger body sizes between 20 and 10 Ma[26]. The increasing efficiency of this feeding form with body size increased pressure towards gigantism, and when ocean conditions supporting large diatoms and large swarming zooplankton arose 5 Ma[66], it selected for the rapid evolution of large body size to better access prey that migrates to depth. Large size subsequently would allow filter feeding to remain efficient, even if ocean conditions developed less favourably for filter feeding at lower body sizes.

Many mammalian lineages have exhibited rapid changes in body-size plans[29]. The confluence of adaptations that facilitate filter feeding with environmental conditions that stimulate large, dense patches of krill probably enabled the evolution of extant ocean giants. Large body size generally allows a more extensive foraging range, a greater sensory-perception distance, lower mass-specific metabolic rates, greater mass-specific lipid stores, lower mass-specific intake needs, decreased predation risk, longer life expectancies and slower paces of life[27,29,39,44,79,80]. Our analysis suggests that an MSC for obligate filter feeding ultimately derives from limitations on volume of water that can be filtered per unit time available for foraging. In turn, the necessity of filter feeders to be large bodied relative to other animals with similar body plans, combined with the increasing efficiency of filter feeding with body size, suggests that filter feeding and gigantism probably co-evolved, with one being necessary to support the other.

Methods

Tag data collection and processing

Our research was conducted in the coastal bays on the western side of the Antarctic Peninsula, specifically focused in Andvord and Paradise bays, previously known to contain high concentrations of both krill and baleen whales including humpback and minke whales. Field work consisted of 24 field days in February/March 2018 and 2019 onboard the ARSV *Laurence M Gould*. Tagging work was done from a 4.8 m aluminium-hulled SOLAS and a 5 m Zodiac Mark V inflatable boat launched from the *Gould*. A 6 m carbon-fibre pole was used to deploy suction-cup-attached video and inertial measurement unit tags manufactured by Customized Animal Tracking Solutions (CATS)[81,82]. All work was conducted under National Marine Fisheries Service permits (no. 23095 and 16111) and Antarctic Conservation Act permits 2020-016, as well as institutional animal care protocols approved by the University of California, Santa Cruz. To compare AMW data with different rorqual species, we additionally analysed krill-feeding humpback whale (Antarctic, US West Coast and South African West Coast) and Northeast Pacific blue whale feeding rates using previously published inertial measurement unit data and animal length measurements[33,48,49]. Within measured blue whales in the published dataset, only 4 met our criteria of feeding for at least 2 h in shallow water to be included in the cross-species comparison of feeding rate, and 13 humpback whales met the criteria. Accordingly, we additionally ran a comparison including all tagged blue whales in our dataset ($n = 100$), assigning them a mean length of 22.6 m (the mean of all measured blue whales from ref. [83]), and assigned unmeasured humpback whales ($n = 40$) a length of 12.8 m[83], increasing those datasets with sufficient shallow feeding hours to 9 and 28 animals, respectively.

Tag accelerometers for all AMW deployments were sampled at 400 Hz, magnetometers and gyroscopes at 50 Hz, and pressure, light, temperature and global positioning system data at 10 Hz. All data were decimated to 10 Hz, tag orientation on the animal was corrected for and animal orientation (pitch, roll, heading) was calculated using custom-written scripts in MATLAB 2014a following ref. [84]. Animal speed for all deployments was determined using the amplitude of tag vibrations[85], and animal positions for the duration of each deployment were estimated from interpolating pseudotracks of the animal between known fast-acquisition global positioning system positions collected by the tags when the whales were at the surface and distributing accumulated error along the track[86]. Lunge-feeding events—the rapid engulfment of a mouthful of prey-laden water followed by subsequent filtration (Supplementary Video 1)—were identified from the tag record (for example, Fig. 1d,e) via the identification of stereotyped manoeuvres, typified by acceleration followed by rapid deceleration[37,81] as the whale is slowed from the engulfed water mass[87].

Animal length

UAS (drones) were launched in concert with tagging effort to collect images suitable for photogrammetry analysis. We used two types of custom hexacopter, the FreeFly Alta 6 and a MikroKopter-based LemHex-44. Both hexacopters contained a two-axis gimbal fitted with a Lightware SF11/C laser altimeter and a Sony Alpha A5100 camera with an APS-C sensor (23.5 × 15.6 mm), 6,000 × 4,000 pixel resolution and either a Sony SEL 50 mm or SEL 35 mm focal length low-distortion lens. We used MorphoMetriX open-source photogrammetry software to measure the total length (in pixels) of each individual, as the tip of the rostrum to the fluke notch[88]. To incorporate photogrammetric uncertainty, we used the Bayesian statistical model and training data described in refs. [25,83], where known-sized objects measured at various altitudes are used as training data to predict the length of each unknown-sized whale. Each individual (up to five length measurements each) was input separately with the training data in the Bayesian statistical model, producing a posterior predictive distribution for length for each individual. We then described the length of each individual by the mean of its posterior predictive distribution and defined measurement uncertainty by constructing 95% highest posterior density intervals[25,83]. UAS images were collected for 18 of 28 total deployments (14 of 24 unique IDs), and body lengths were determined photogrammetrically (Extended Data Table 1).

To estimate length for the remaining 10 whales, a relationship between estimated buccal cavity length (VGB_{est}) and body length was calculated for 12 deployments with both UAS measurements and sufficient video data during engulfment to calculate VGB_{est} (Fig. 1a). VGB_{est} was calculated as the integral of speed over the time interval from mouth opening to mouth closing (Fig. 3a), as in ref. [81]. This distance, the distance travelled during engulfment, is presumed to relate to the ventral groove

blubber that starts at the tip of the mouth and runs down the belly of rorqual whales[81]. Mouth opening was defined as the first appearance in the frame of any part of the rostrum during engulfment (Supplementary Video 2). Mouth closing was defined as the first video frame when that same region disappears from view. Up to 30 lunges with good visibility were selected for each whale. For all whales except bb190228-55b (deployment 18 in Fig. 1a), camera position was similar during the lunges selected: facing forward and located near the dorsal ridge with a good view of the mouth forward of the nares. For bb190228-55b, the tag was located very close to the nares, leading to a longer determination of engulfment duration that probably skewed the estimate of VGB length. This same whale was tagged subsequently (bb190306-52, deployment 27) resulting in a more expected VGB_{est}. For purposes of calculating the line of best fit, deployment 18 was therefore excluded. For the remaining whales, log(VGB_{est}) was regressed against log(total length) estimated from UAS images with R^2 of 0.97 (Fig. 1a), giving confidence that the regression line could be used predictively to assign lengths to the remaining 10 whales that had good views of engulfment but did not have corresponding UAS imagery (Extended Data Table 1).

General analysis

Animals may start or stop foraging efforts due to prey availability, satiation or non-prey-related factors (for example, social behaviour, anti-predator behaviour, migration, fatigue). To study the influence of body size and environmental restrictions on feeding rate, we first restricted our analysis to time periods of active foraging[89]. Rorqual whale feeding behaviour is a constant optimization problem balancing resource acquisition at depth with oxygen acquisition at the surface[90,91]. Stereotypical behaviour consists of diving from the surface, performing from one to ten or more discrete lunges, then surfacing for one to a dozen or more breaths and then diving to forage again. We categorized foraging bouts as periods of consecutive dives containing at least one lunge without a prolonged break between feeding dives. To determine 'prolonged', we applied the same method used for blue whales and humpback whales in ref. [48] to our AMW data. This method examines the distributions of surface intervals between the end of a feeding dive and the start of the next dive (feeding or not). Surface interval for all whales demonstrated clear bi- or multimodal distributions (Extended Data Fig. 7), so Gaussian curves were fitted (using the fitgmdist function in MATLAB 2014a), and the first set of curves that best matched the shape of the distribution was selected. The surface interval equivalent to the final mean + 3 s.d. in the bulk of the data was chosen as the value to separate feeding behaviour into foraging bouts. Feeding dives separated by more than this inter-bout interval (6 min) were considered to be part of separate foraging bouts. Feeding rates (λ_f in lunges h^{-1} within foraging bouts) were determined for each whale by dividing the number of lunges by the total duration of all foraging bouts. For humpback and blue whales, 5.5 min was used as the threshold between foraging bouts (as determined in ref. [48] using the same method).

Feeding rates were additionally differentiated by depth zone and by diel period. Foraging dives <35 m were classified as shallow, and dives >35 m were classified as deep. This threshold (~4 body lengths) was chosen based on the mean maximum difference in depth from the first lunge to the last lunge in a dive by a humpback whale (that is, the depth differential through which a whale would be expected to forage)[33]. The same procedure for AMW resulted in a depth differential of 40 m, while for blue whales it was 44 m[33]. The humpback whale threshold was chosen for consistency across species, because all species had similar values, and the effect of slight variation in choice of threshold was small (AMW in our dataset performed 5,018 foraging dives <35 m and 5,083 foraging dives <40 m).

Diel period (day/night/twilight) was determined from the angular sun position at a given location and time using the MATLAB package Sunrise/Sunset (https://www.mathworks.com/matlabcentral/fileexchange/55509-sunrise-sunset). Twilight was defined as the period when solar elevation was 0–6° below the horizon and was determined in order to exclude those transitional time periods from daylight and nighttime hours. Feeding rates during daylight and night were calculated separately for all three species. Given the limited sample size of twilight feeding, for daily intake rates calculated in Extended Data Fig. 8, daytime and nighttime rates and proportion of time feeding were averaged for the duration of twilight periods.

Slopes of regression lines for the relationship between body length and feeding rate (Fig. 2e–j) were calculated using the fitlm.m function in MATLAB 2020b, and slopes were compared with allometrically predicted slopes using *F*-tests via the MATLAB function coefTest.m. In Fig. 2, 'slope CI' refers to 95% confidence intervals.

Constraints on λ_f

To investigate the relationship of biomechanical constraints on feeding rate with body size, we calculated the filter time, engulfment time and approach time for 30 randomly selected lunges from all 23 measured AMW. We limited lunges to those >20 m depth (to remove the effects of surface forces from kinematic data) that were not the first or last lunge in a dive (to avoid the effects of dive descent and ascent, respectively). Approach time was determined as the start of the acceleration period (Fig. 3a) until the start of engulfment. Engulfment time for the selected lunges was determined as the start of estimated mouth opening (beginning of deceleration) to estimated mouth closing (end of deceleration). These definitions were first determined in blue and humpback whales via video analysis[77,81] and were confirmed for AMW when video was available (Fig. 3a). Filter time was identified from mouth closing until the initiation of fluking post-lunge as in ref. [37]. The environmental constraint of search time between lunges was calculated as ILI minus filter time and approach time.

To calculate the physiological constraint of dive time and bottom time, dives were first identified using the finddives.m tool from animaltags.org as departures from the surface greater than 5 m. The surface interval on either side of a feeding dive was identified as the time between the end of one dive and the start of the next, for feeding dives within the same foraging bout. Descent (and ascent) periods were defined with one endpoint at the start (end) of a dive, and the other at the earlier (later) of the following: the first (last) time the animal's pitch is >(<)0, or 5 s before (after) the first (last) lunge in a dive.

Maximum feeding rate (λ_{f_max}, in lunges h^{-1}) for an AMW of length *L* was calculated based on the above constraints for each diel period (*D* = day or night) as a function of length as:

$$\lambda_{f\_max\_D} = \frac{3{,}600}{search\_D(L)+filt\_D(L)+engulf\_D(L)+accel\_D(L)} \times bottomratio\_D(L) \quad (3)$$

where search, filt, engulf and accel (in s), and bottomratio (unitless), are the relationships of *L* to search time, filter time, engulfment time, acceleration time (Fig. 3c,d) and bottom ratio (Fig. 4) for each diel period, respectively.

Reporting summary

Further information on research design is available in the Nature Portfolio Reporting Summary linked to this article.

Data availability

The datasets analysed during the current study are available at Stanford's digital repository, https://purl.stanford.edu/pm378wm1385. This deposit includes processed bio-logging data describing animal orientation, motion and position; video data used to calculate engulfment timing; audited feeding data including indices of identified foraging events and start and end points of feeding bouts; summarized foraging data for all species; and aerial imagery and length analysis.

Code availability

Custom code and a wiki tutorial for processing raw tag data into animal orientation, motion and position is available in ref. [84] and directly at https://github.com/wgough/CATS-Methods-Materials.

References

1. Dove, A. D. & Pierce, S. J. *Whale Sharks: Biology, Ecology, and Conservation* (CRC Press, 2021).
2. Friedman, M. et al. 100-million-year dynasty of giant planktivorous bony fishes in the Mesozoic seas. *Science* **327**, 990–993 (2010).
3. Friedman, M. Parallel evolutionary trajectories underlie the origin of giant suspension-feeding whales and bony fishes. *Proc. R. Soc. B* https://doi.org/10.1098/rspb.2011.1381 (2011).
4. Sanderson, S. L. & Wassersug, R. in *The Skull: Functional and Evolutionary Mechanisms* Vol. 3 (eds Hanken, J. & Hall, B. K.) 37–112 (Univ. Chicago Press, 1993).
5. Rowat, D. & Brooks, K. A review of the biology, fisheries and conservation of the whale shark *Rhincodon typus*. *J. Fish Biol.* **80**, 1019–1056 (2012).
6. Pimiento, C., Cantalapiedra, J. L., Shimada, K., Field, D. J. & Smaers, J. B. Evolutionary pathways toward gigantism in sharks and rays. *Evolution* **73**, 588–599 (2019).
7. Stiefel, K. M. Evolutionary trends in large pelagic filter-feeders. *Hist. Biol.* **33**, 1477–1488 (2021).
8. Goldbogen, J. & Madsen, P. The largest of August Krogh animals: physiology and biomechanics of the blue whale revisited. *Comp. Biochem. Physiol. A* **254**, 110894 (2021).
9. Jørgensen, C. B. Quantitative aspects of filter feeding in invertebrates. *Biol. Rev.* **30**, 391–453 (1955).
10. Radke, R. J. & Kahl, U. Effects of a filter-feeding fish [silver carp, *Hypophthalmichthys molitrix* (Val.)] on phyto-and zooplankton in a mesotrophic reservoir: results from an enclosure experiment. *Freshw. Biol.* **47**, 2337–2344 (2002).
11. Schiemer, F. in *Perspectives in Tropical Limnology* (eds Schiemer, F. & Boland, K.T.) 65–76 (SPB Academic Publishing, 1996).
12. Carey, N. & Goldbogen, J. A. Kinematics of ram filter feeding and beat-glide swimming in the northern anchovy *Engraulis mordax*. *J. Exp. Biol.* **220**, 2717–2725 (2017).
13. Haines, G. E. & Sanderson, S. L. Integration of swimming kinematics and ram suspension feeding in a model American paddlefish, *Polyodon spathula*. *J. Exp. Biol.* **220**, 4535–4547 (2017).
14. Paig-Tran, E. M., Kleinteich, T. & Summers, A. P. The filter pads and filtration mechanisms of the devil rays: variation at macro and microscopic scales. *J. Morphol.* **274**, 1026–1043 (2013).
15. Jacobsen, I. P. & Bennett, M. B. A comparative analysis of feeding and trophic level ecology in stingrays (Rajiformes; Myliobatoidei) and electric rays (Rajiformes: Torpedinoidei). *PLoS ONE* **8**, e71348 (2013).
16. Ellis, J. Occurrence of pelagic stingray *Pteroplatytrygon violacea* (Bonaparte, 1832) in the North Sea. *J. Fish Biol.* **71**, 933–937 (2007).
17. Werth, A. J. & Potvin, J. Baleen hydrodynamics and morphology of cross-flow filtration in balaenid whale suspension feeding. *PLoS ONE* **11**, e0150106 (2016).
18. Orton, L. S. & Brodie, P. F. Engulfing mechanics of fin whales. *Can. J. Zool.* **65**, 2898–2907 (1987).
19. Shadwick, R. E., Goldbogen, J. A., Potvin, J., Pyenson, N. D. & Vogl, A. W. Novel muscle and connective tissue design enables high extensibility and controls engulfment volume in lunge-feeding rorqual whales. *J. Exp. Biol.* **216**, 2691–2701 (2013).
20. Shadwick, R. E., Goldbogen, J. A., Pyenson, N. D. & Whale, J. C. Structure and function in the lunge feeding apparatus: mechanical properties of the fin whale mandible. *Anat. Rec.* **300**, 1953–1962 (2017).
21. Werth, A. J., Ito, H. & Ueda, K. Multiaxial movements at the minke whale temporomandibular joint. *J. Morphol.* **281**, 402–412 (2020).
22. Lambertsen, R., Ulrich, N. & Straley, J. Frontomandibular stay of Balaenopteridae: a mechanism for momentum recapture during feeding. *J. Mammal.* **76**, 877–899 (1995).
23. Pyenson, N. D. et al. Discovery of a sensory organ that coordinates lunge feeding in rorqual whales. *Nature* **485**, 498–501 (2012).
24. Goldbogen, J. A. et al. How baleen whales feed: the biomechanics of engulfment and filtration. *Annu. Rev. Mar. Sci.* **9**, 367–386 (2017).
25. Bierlich, K. C. et al. A Bayesian approach for predicting photogrammetric uncertainty in morphometric measurements derived from drones. *Mar. Ecol. Prog. Ser.* **673**, 193–210 (2021).
26. Slater, G. J., Goldbogen, J. A. & Pyenson, N. D. Independent evolution of baleen whale gigantism linked to Plio-Pleistocene ocean dynamics. *Proc. R. Soc. B* **284**, 20170546 (2017).
27. Lockyer, C. Growth and energy budgets of large baleen whales from the Southern Hemisphere. *Food Agric. Organ.* **3**, 379–487 (1981).
28. Mackintosh, A. & Wheeler, J. Southern blue and fin whales. *Discover. Rep.* **1**, 257–540 (1929).
29. Smith, F. A. & Lyons, S. K. How big should a mammal be? A macroecological look at mammalian body size over space and time. *Phil. Trans. R. Soc. B* **366**, 2364–2378 (2011).
30. Gearty, W., McClain, C. R. & Payne, J. L. Energetic tradeoffs control the size distribution of aquatic mammals. *Proc. Natl Acad. Sci. USA* **115**, 4194–4199 (2018).
31. Lockyer, C. Body weights of some species of large whales. *ICES J. Mar. Sci.* **36**, 259–273 (1976).
32. Goldbogen, J. A. Physiological constraints on marine mammal body size. *Proc. Natl Acad. Sci. USA* **115**, 3995–3997 (2018).
33. Goldbogen, J. A. et al. Why whales are big but not bigger: physiological drivers and ecological limits in the age of ocean giants. *Science* **366**, 1367–1372 (2019).
34. Cade, D. E. et al. Social exploitation of extensive, ephemeral, environmentally controlled prey patches by super-groups of rorqual whales. *Anim. Behav.* **182**, 251–266 (2021).
35. Goldbogen, J. A. et al. Scaling of lunge-feeding performance in rorqual whales: mass-specific energy expenditure increases with body size and progressively limits diving capacity. *Funct. Ecol.* **26**, 216–226 (2012).
36. Kahane-Rapport, S. R. & Goldbogen, J. A. Allometric scaling of morphology and engulfment capacity in rorqual whales. *J. Morphol.* **279**, 1256–1268 (2018).
37. Kahane-Rapport, S. R. et al. Lunge filter feeding biomechanics constrain rorqual foraging ecology across scale. *J. Exp. Biol.* https://doi.org/10.1242/jeb.224196 (2020).
38. McNab, B. K. Complications inherent in scaling the basal rate of metabolism in mammals. *Q. Rev. Biol.* **63**, 25–54 (1988).
39. Boyd, I. in *Marine Mammal Biology: An Evolutionary Approach* (ed. Hoelzel, A. R.) 247–277 (Blackwell Science Ltd, 2002).
40. Kleiber, M. Body size and metabolism. *Hilgardia* **6**, 315–353 (1932).
41. West, G. B., Brown, J. H. & Enquist, B. J. A general model for the origin of allometric scaling laws in biology. *Science* **276**, 122–126 (1997).
42. Corkeron, P. J. & Connor, R. C. Why do baleen whales migrate? *Mar. Mamm. Sci.* **15**, 1228–1245 (1999).
43. Lockyer, C. Review of baleen whale (Mysticeti) reproduction and implications for management. *Rep. Int. Whal. Commn* **6**, 27–50 (1984).
44. Lockyer, C. All creatures great and smaller: a study in cetacean life history energetics. *J. Mar. Biol. Assoc. UK* **87**, 1035–1045 (2007).
45. Frazer, J. & Huggett, A. S. G. Specific foetal growth rates of cetaceans. *J. Zool.* **169**, 111–126 (1973).

46. Zhou, M. & Dorland, R. D. Aggregation and vertical migration behavior of *Euphausia superba*. *Deep Sea Res. II* **51**, 2119–2137 (2004).
47. Gough, W. T. et al. Scaling of swimming performance in baleen whales. *J. Exp. Biol.* **222**, jeb204172 (2019).
48. Cade, D. E. et al. Predator-scale spatial analysis of intra-patch prey distribution reveals the energetic drivers of rorqual whale super group formation. *Funct. Ecol.* **35**, 894–908 (2021).
49. Gough, W. T. et al. Scaling of oscillatory kinematics and Froude efficiency in baleen whales. *J. Exp. Biol.* **224**, jeb237586 (2021).
50. Croll, D. A., Kudela, R. & Tershy, B. R. in *Whales, Whaling, and Ocean Ecosystems* (eds Estes, J. A. et al.) Ch. 16 (Univ. California Press, 2006).
51. Woodward, B. L., Winn, J. P. & Fish, F. E. Morphological specializations of baleen whales associated with hydrodynamic performance and ecological niche. *J. Morphol.* **267**, 1284–1294 (2006).
52. Webb, P. W. & De Buffrénil, V. Locomotion in the biology of large aquatic vertebrates. *Trans. Am. Fish. Soc.* **119**, 629–641 (1990).
53. Acevedo-Gutiérrez, A., Croll, D. & Tershy, B. High feeding costs limit dive time in the largest whales. *J. Exp. Biol.* **205**, 1747–1753 (2002).
54. Goldbogen, J. A. et al. Mechanics, hydrodynamics and energetics of blue whale lunge feeding: efficiency dependence on krill density. *J. Exp. Biol.* **214**, 131–146 (2011).
55. Potvin, J., Cade, D. E., Werth, A. J., Shadwick, R. E. & Goldbogen, J. A. Rorqual lunge-feeding energetics near and away from the kinematic threshold of optimal efficiency. *Integr. Org. Biol.* **3**, obab005 (2021).
56. Pyenson, N. D. The ecological rise of whales chronicled by the fossil record. *Curr. Biol.* **27**, R558–R564 (2017).
57. Williams, T. M. in *Whales, Whaling, and Ocean Ecosystems* (eds Estes, J. A. et al.) Ch. 15 (Univ. California Press, 2006).
58. Tackaberry, J. E. et al. From a calf's perspective: humpback whale nursing behavior on two US feeding grounds. *PeerJ* **8**, e8538 (2020).
59. Huang, S.-L., Chou, L.-S. & Ni, I.-H. Comparable length at weaning in cetaceans. *Mar. Mamm. Sci.* **25**, 875–887 (2009).
60. Rice, D. *Marine Mammals of the World: Systematics and Distribution* (Society for Marine Mammalogy Special Publication, 1998).
61. McNamara, J. M. & Houston, A. I. The effect of a change in foraging options on intake rate and predation rate. *Am. Nat.* **144**, 978–1000 (1994).
62. Mittelbach, G. G. Foraging efficiency and body size: a study of optimal diet and habitat use by bluegills. *Ecology* **62**, 1370–1386 (1981).
63. Robbins, C. T. et al. Optimizing protein intake as a foraging strategy to maximize mass gain in an omnivore. *Oikos* **116**, 1675–1682 (2007).
64. Werth, A. J. et al. Filtration area scaling and evolution in mysticetes: trophic niche partitioning and the curious cases of sei and pygmy right whales. *Biol. J. Linn. Soc.* **125**, 264–279 (2018).
65. Leslie, M. S., Peredo, C. M. & Pyenson, N. D. *Norrisanima miocaena*, a new generic name and redescription of a stem balaenopteroid mysticete (Mammalia, Cetacea) from the Miocene of California. *PeerJ* **7**, e7629 (2019).
66. Marx, F. G. & Uhen, M. D. Climate, critters, and cetaceans: Cenozoic drivers of the evolution of modern whales. *Science* **327**, 993–996 (2010).
67. Perrin, W. F. Why are there so many kinds of whales and dolphins? *Bioscience* **41**, 460–462 (1991).
68. Kot, B. W., Sears, R., Zbinden, D., Borda, E. & Gordon, M. S. Rorqual whale (Balaenopteridae) surface lunge-feeding behaviors: standardized classification, repertoire diversity, and evolutionary analyses. *Mar. Mamm. Sci.* **30**, 1335–1357 (2014).
69. Segre, P. S. et al. Scaling of maneuvering performance in baleen whales: larger whales outperform expectations. *J. Exp. Biol.* **225**, jeb243224 (2022).
70. Kawamura, A. A review of food of balaenopterid whales. *Sci. Rep. Whales Res. Inst.* **32**, 155–197 (1980).
71. Iwata, T. et al. Tread-water feeding of Bryde's whales. *Curr. Biol.* **27**, R1154–R1155 (2017).
72. McMillan, C. J., Towers, J. R. & Hildering, J. The innovation and diffusion of "trap-feeding," a novel humpback whale foraging strategy. *Mar. Mamm. Sci.* **35**, 779–796 (2019).
73. Robbins, J. & Mattila, D. *Estimating Humpback Whale (*Megaptera novaeangliae*) Entanglement Rates on the Basis of Scar Evidence* (Northeast Fisheries Science Center, 2004).
74. Horwood, J. in *Encyclopedia of Marine Mammals* 2nd edn (eds Wursig, B et al.) 1001–1003 (Elsevier, 2009).
75. Haug, T., Lindstrøm, U. & Nilssen, K. T. Variations in minke whale (*Balaenoptera acutorostrata*) diet and body condition in response to ecosystem changes in the Barents Sea. *Sarsia* **87**, 409–422 (2002).
76. García-Vernet, R., Borrell, A., Víkingsson, G., Halldórsson, S. D. & Aguilar, A. Ecological niche partitioning between baleen whales inhabiting Icelandic waters. *Prog. Oceanogr.* **199**, 102690 (2021).
77. Cade, D. E., Carey, N., Domenici, P., Potvin, J. & Goldbogen, J. A. Predator-informed looming stimulus experiments reveal how large filter feeding whales capture highly maneuverable forage fish. *Proc. Natl Acad. Sci. USA* **117**, 472–478 (2020).
78. Deméré, T. A., McGowen, M. R., Berta, A. & Gatesy, J. Morphological and molecular evidence for a stepwise evolutionary transition from teeth to baleen in mysticete whales. *Syst. Biol.* **57**, 15–37 (2008).
79. Stafford, K. M., Fox, C. G. & Clark, D. S. Long-range acoustic detection and localization of blue whale calls in the northeast Pacific Ocean. *J. Acoust. Soc. Am.* **104**, 3616–3625 (1998).
80. Totterdell, J. A. et al. The first three records of killer whales (*Orcinus orca*) killing and eating blue whales (*Balaenoptera musculus*). *Mar. Mamm. Sci.* **38**, 1286–1301 (2022).
81. Cade, D. E., Friedlaender, A. S., Calambokidis, J. & Goldbogen, J. A. Kinematic diversity in rorqual whale feeding mechanisms. *Curr. Biol.* **26**, 2617–2624 (2016).
82. Goldbogen, J. A. et al. Using digital tags with integrated video and inertial sensors to study moving morphology and associated function in large aquatic vertebrates. *Anat. Rec.* **300**, 1935–1941 (2017).
83. Bierlich, K. et al. Comparing uncertainty associated with 1-, 2-, and 3D aerial photogrammetry-based body condition measurements of baleen whales. *Front. Mar. Sci.* **8**, 1729 (2021).
84. Cade, D. E. et al. Tools for integrating inertial sensor data with video bio-loggers, including estimation of animal orientation, motion, and position. *Anim. Biotelemetry* https://doi.org/10.1186/s40317-021-00256-w (2021).
85. Cade, D. E., Barr, K. R., Calambokidis, J., Friedlaender, A. S. & Goldbogen, J. A. Determining forward speed from accelerometer jiggle in aquatic environments. *J. Exp. Biol.* **221**, jeb170449 (2018).
86. Wilson, R. P. et al. All at sea with animal tracks; methodological and analytical solutions for the resolution of movement. *Deep Sea Res. II* **54**, 193–210 (2007).
87. Potvin, J., Cade, D. E., Werth, A. J., Shadwick, R. E. & Goldbogen, J. A. A perfectly inelastic collision: bulk prey engulfment by baleen whales and dynamical implications for the world's largest cetaceans. *Am. J. Phys.* **88**, 851–863 (2020).
88. Torres, W. I. & Bierlich, K. MorphoMetriX: a photogrammetric measurement GUI for morphometric analysis of megafauna. *J. Open Source Softw.* **5**, 1825 (2020).
89. Suter, H. & Houston, A. I. How to model optimal group size in social carnivores. *Am. Nat.* **197**, 473–485 (2021).

90. Hazen, E. L., Friedlaender, A. S. & Goldbogen, J. A. Blue whale (*Balaenoptera musculus*) optimize foraging efficiency by balancing oxygen use and energy gain as a function of prey density. *Sci. Adv.* **1**, e1500469 (2015).
91. Doniol-Valcroze, T., Lesage, V., Giard, J. & Michaud, R. Optimal foraging theory predicts diving and feeding strategies of the largest marine predator. *Behav. Ecol.* **22**, 880–888 (2011).
92. Gough, W. T. et al. Fast and furious: energetic tradeoffs and scaling of high-speed foraging in rorqual whales. *Integr. Org. Biol.* **4**, obac038 (2022).
93. Laws, R. M. The ecology of the Southern Ocean. *Am. Sci.* **73**, 26–40 (1985).
94. Brown, S. & Lockyer, C. in *Antarctic Ecology* Vol. 2 (ed. Laws, R. M.) (Academic Press, 1984).
95. Peters, R. H. *The Ecological Implications of Body Size* Vol. 2 Ch. 7 (Cambridge Univ. Press, 1986).
96. Rall, B. C. et al. Universal temperature and body-mass scaling of feeding rates. *Phil. Trans. R. Soc. B* **367**, 2923–2934 (2012).
97. Evans, E. & Miller, D. Comparative nutrition, growth and longevity. *Proc. Nutr. Soc.* **27**, 121–129 (1968).
98. Farlow, J. O. A consideration of the trophic dynamics of a Late Cretaceous large-dinosaur community (Oldman Formation). *Ecology* **57**, 841–857 (1976).
99. Harestad, A. S. & Bunnel, F. Home range and body weight – a reevaluation. *Ecology* **60**, 389–402 (1979).
100. Schoener, T. W. Sizes of feeding territories among birds. *Ecology* **49**, 123–141 (1968).
101. Calder, W. A. in *Avian Energetics* (ed. Paynter, R. A.) 86–151 (Nuttall Ornithological Club, 1974).
102. Savage, V. M., Deeds, E. J. & Fontana, W. Sizing up allometric scaling theory. *PLoS Comp. Biol.* **4**, e1000171 (2008).
103. Kolokotrones, T., Savage, V., Deeds, E. J. & Fontana, W. Curvature in metabolic scaling. *Nature* **464**, 753–756 (2010).
104. Hudson, L. N., Isaac, N. J. & Reuman, D. C. The relationship between body mass and field metabolic rate among individual birds and mammals. *J. Anim. Ecol.* **82**, 1009–1020 (2013).

Acknowledgements

This work was primarily funded with NSF OPP grant no. 1643877, with additional funding from ONR YIP grant no. N000141612477 and Stanford University's Terman Fellowship. This work was authorized under NMFS permits 16111 and 23095 and ACA permit 2020-016. We wish to thank J. Dale, C. Taylor, E. Levy and P. Gray for their contributions to data collection. A special thanks is also extended to the scientists and crew of the *Lawrence M Gould*, especially E. Hutt and the marine techs.

Author contributions

D.E.C. led the study, performed all statistical tests and led the writing of the manuscript. D.E.C., S.R.K.-R., W.T.G., J.A.G. and A.S.F. designed methodology. D.E.C., S.R.K.-R., W.T.G and J.M.J.L. analysed video and accelerometry data. K.C.B. analysed aerial photogrammetry data. D.E.C., S.R.K.-R., J.M.J.L., K.C.B., J.C., D.W.J., J.A.G. and A.S.F. collected field data. J.C., D.W.J., J.A.G. and A.S.F. acquired funding, provided resources and supervised the work. All authors contributed to review and editing.

Competing interests

The authors declare no competing interests.

Additional information

Extended data is available for this paper at https://doi.org/10.1038/s41559-023-01993-2.

Supplementary information The online version contains supplementary material available at https://doi.org/10.1038/s41559-023-01993-2.

Correspondence and requests for materials should be addressed to David E. Cade.

Peer review information *Nature Ecology & Evolution* thanks William Gearty, Rochelle Constantine, Brian Kot and the other, anonymous, reviewer(s) for their contribution to the peer review of this work. Peer reviewer reports are available.

https://doi.org/10.1038/s41559-023-01993-2

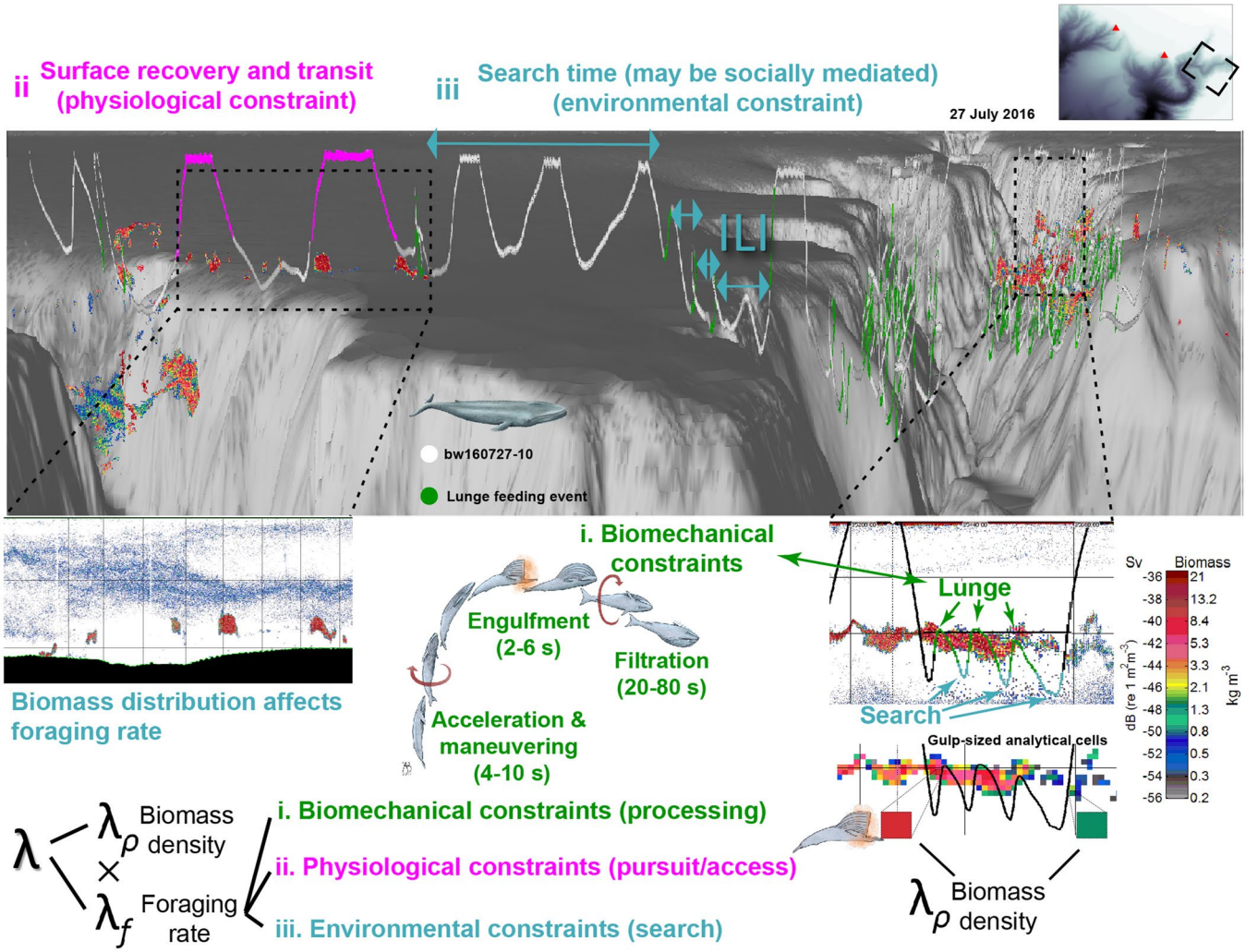

Extended Data Fig. 1 | Constraints on intake rate in rorqual whales. First published in[34], reproduced with permission. Three-dimensional plot crafted in Echoview v.10 using a 10x vertical exaggeration and 120 kHz data, with the spatially matched track of a tagged blue whale. Biomass estimated as in[48]. Two-dimensional plots are temporally linked echosounding data with the tagged whale's depth profile. Illustrations © Alex Boersma.

https://doi.org/10.1038/s41559-023-01993-2

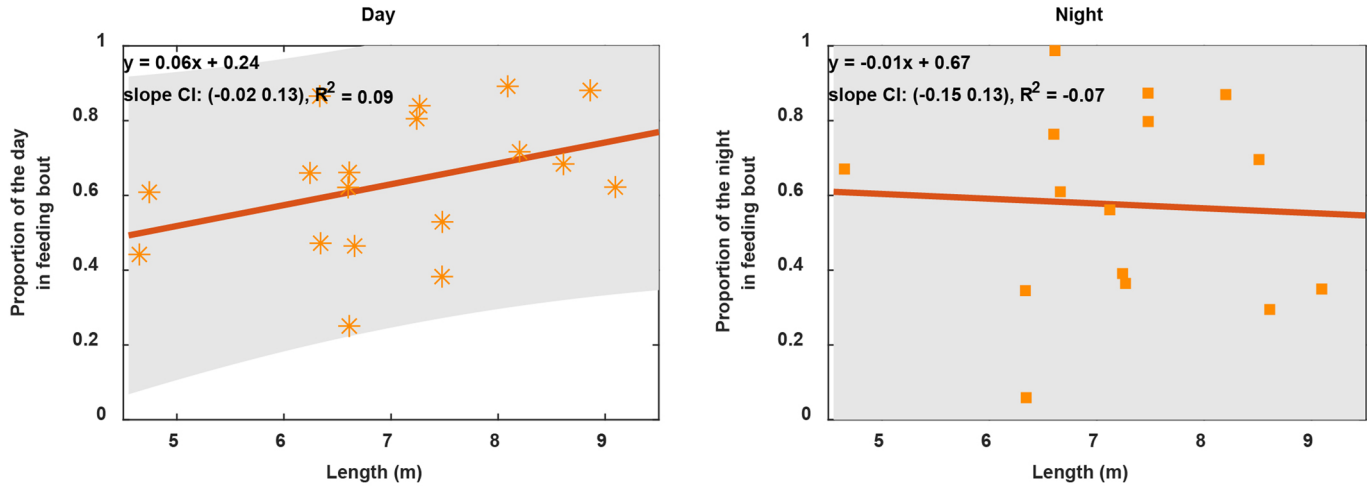

Extended Data Fig. 2 | Proportion of diel periods spent feeding. Proportion of diel periods spent feeding (deployments with at least 4 hours of data in corresponding diel period).

https://doi.org/10.1038/s41559-023-01993-2

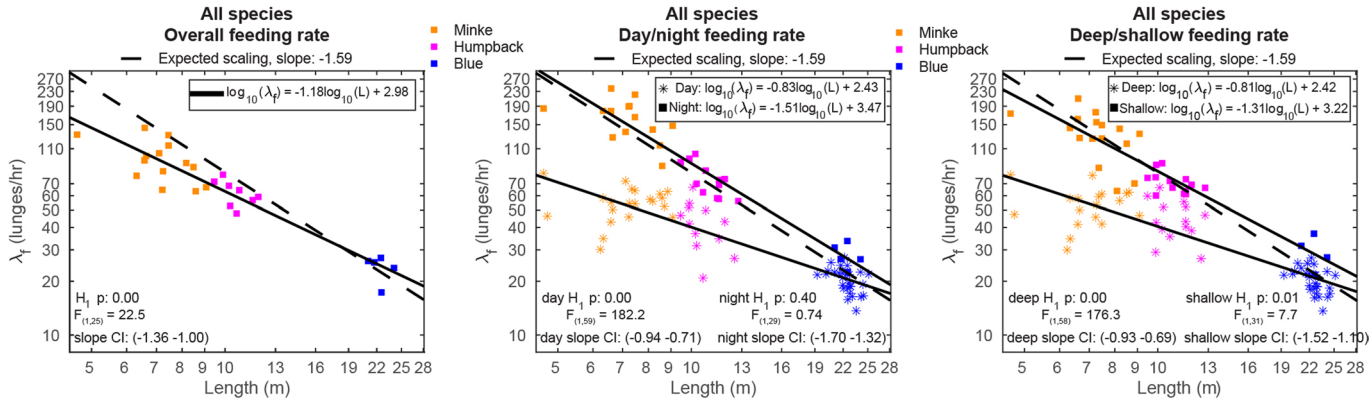

Extended Data Fig. 3 | Regressions of feeding rate on length, using only measured whales. Regressions of feeding rate using only measured blue and humpback whales. Shallow feeding slope is slightly shallower, other differences are non-significant from the regressions in Fig. 2H-J. Slope 95% confidence intervals (CI) *and F-statistics* are displayed, p-values are for the *2-sided F*-test that the indicated regression has a slope different than the expected scaling slope. Both axes are log scales.

https://doi.org/10.1038/s41559-023-01993-2

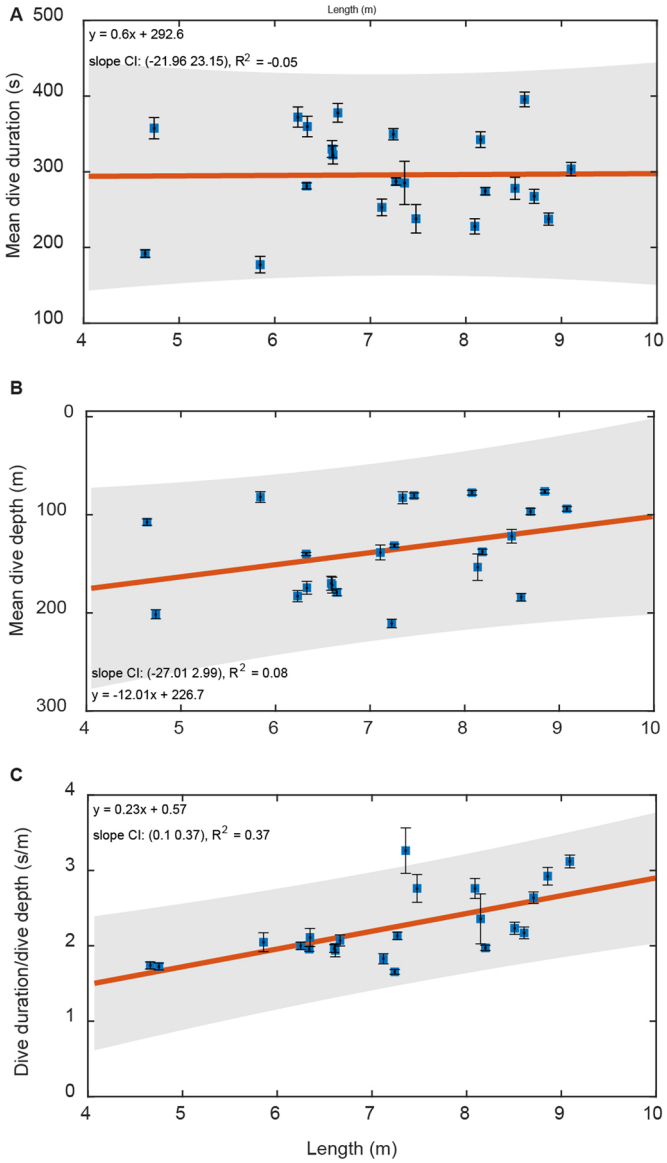

Extended Data Fig. 4 | Relationship of dive behavior to body length. Lack of relationship between A) mean dive duration or B) mean dive depth and body length in AMW for daytime dives. Error bars are standard error. C) Mean dive time relative to dive depth, as a function of length, for daytime dives > 70 m. Error bars are standard error. Sample sizes listed in Extended Data Table 1.

https://doi.org/10.1038/s41559-023-01993-2

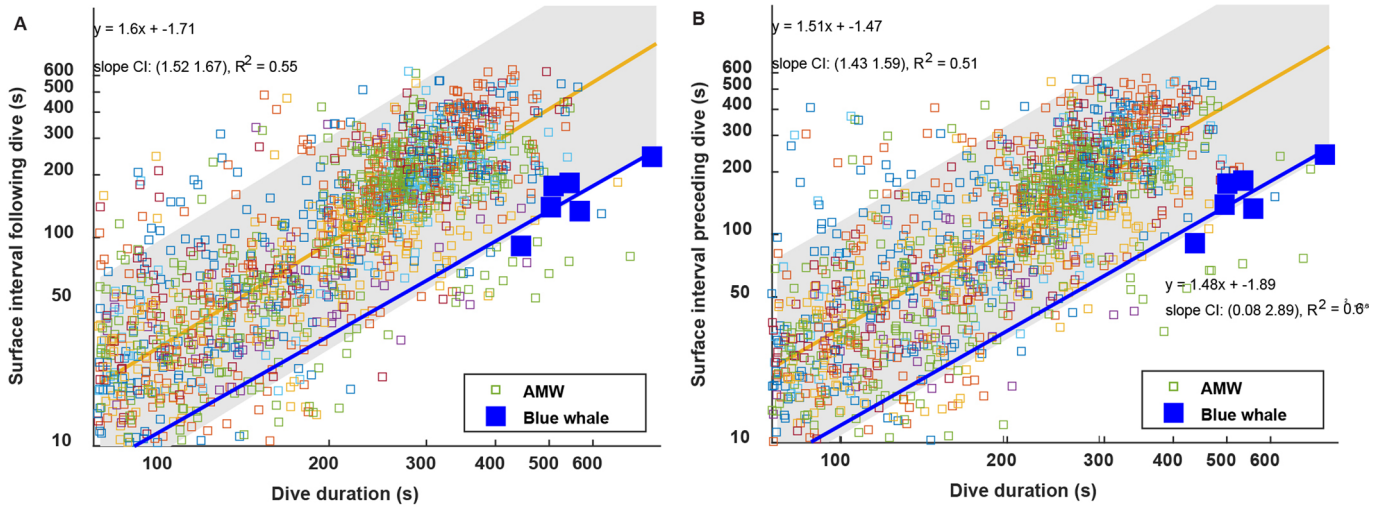

Extended Data Fig. 5 | Dive interval compared to dive duration. AMW surface interval increases with foraging dive duration. Colors represent individual animals. Shown is data for foraging dives > 100 s and with surface intervals > 10 s. Blue whale data reproduced from Fig. 2 in[53]. A) Surface interval between a foraging dive and the following foraging dive (> 35 m), n = 3158 dives. B) Surface interval between a foraging dive and the preceding foraging dive, n = 3147 dives.

https://doi.org/10.1038/s41559-023-01993-2

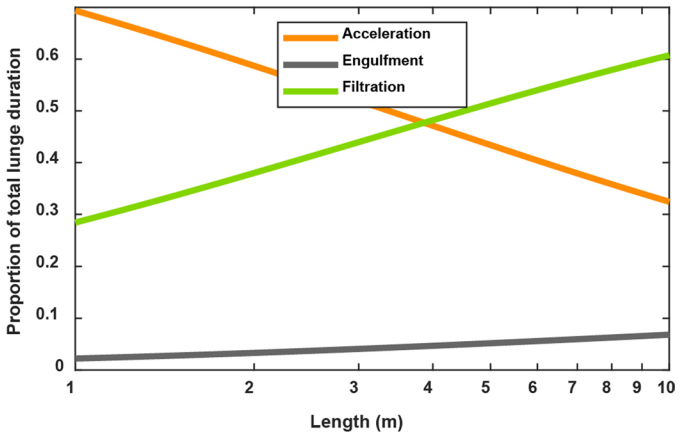

Extended Data Fig. 6 | Proportion of total lunge duration taken up by each component of lunge feeding. Proportion of total lunge duration taken up by each component of lunge feeding. Filtration, the component with the strongest relationship to length, demonstrates a rapidly reduction in its effect on total lunge time (and maximum lunge rate) as size decreases.

https://doi.org/10.1038/s41559-023-01993-2

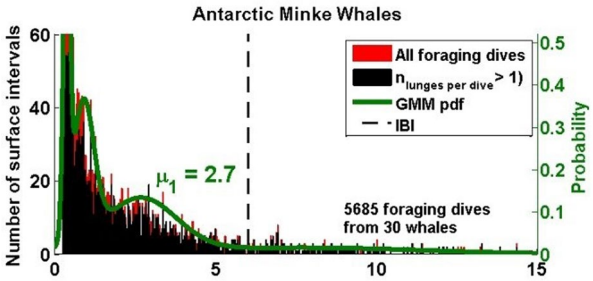

Extended Data Fig. 7 | Estimation of divisions between foraging bouts. Surface interval between foraging dives for AMW. Black bars are surface intervals from foraging dives with at least 2 lunges until the next foraging dive. Red is the surface intervals for all foraging dives. The surface interval duration corresponding to the mean of the largest fitted Gaussian curve in the bulk of the data + 3 *SD* was used to differentiate "foraging bouts." That is, a "foraging bout" was defined as the combined duration of all dives where the surface interval between dives with foraging effort was less than six minutes (the dashed vertical bar). The duration of a foraging bout was thus defined from the start of the first dive to six minutes after the last foraging dive. See[48] for additional justification for this method in blue and humpback whales.

https://doi.org/10.1038/s41559-023-01993-2

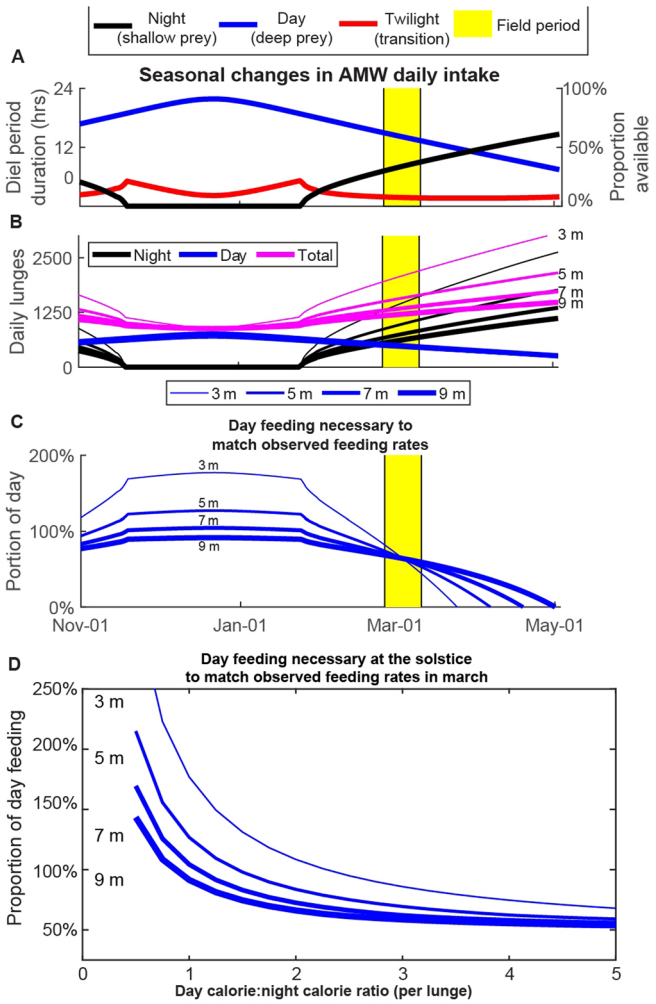

Extended Data Fig. 8 | Seasonal changes in predicted Antarctic minke whale (AMW). Seasonal changes in predicted Antarctic minke whale (AMW) daily intake over a six-month feeding season. A) Day/night lengths at the field site (64.8°S, 62.7°W). The period of no darkness lasts from Nov 19 to Jan 24. The results of this model could also be interpreted as the proportion of shallow or deep lunges available at a given point in time. B) Day, night and total lunges assuming the observed feeding rates during the field season are maintained as well as the observed portion of the day (64%) and night (57%) spent feeding. Solid lines are prediction from regression (Fig. 2F); for the theoretical 3 m whale, this is an extension past observed points. C) The portion of available daylight that an AMW would have to feed to match the mean total daily feeding rates we observed in late Feb/early Mar. Whales 7 m and larger could match the observed feeding rates during peak summer even if prey conditions didn't change, but whales 5 m and smaller would require shallower daytime prey. In all cases, twilight feeding rates were assumed to be the corresponding mean of daytime and nighttime feeding rates. D) The proportion of daylight hours a whale of different lengths would have to spend feeding at the summer solstice to match the total intake observed in Feb/Mar, given the indicated day/night ratio of caloric value per lunge.

https://doi.org/10.1038/s41559-023-01993-2

Extended Data Table 1 | Total length (L) and feeding rate (λ_f) information summarized by individual

																		Fig 3b		Fig 4			ED Fig 4		
Deployment ID	Deployment Number	VGB_{est}			L_{VGBest}	L_{UAS}	95% high posterior density interval		L	Mass	λ_f	Day λ_f	Night λ_f	Day hours	Night hours	Twilight hours	number of dives		number of dives			number of dives	Deployment Location	
																	day	night	< 35 m	35-100 m	> 100 m	> 70 m		
spYYMMDD-tag#		mean (m)	std	n	m	m			m	10^3 kg	lunges/hr	lunges/hr	lunges/hr	hr	hr	hr	n	n	n	n	n	n	Lat (°S)	Long (°W)
bb180227-45	1	3.47	0.66	30	7.48	—	—	—	7.48	5.7	112.5	53.5	220.8	20.1	7.5	2.0	75	214	50	0	0	0	-64.8277	-62.6269
bb180228-42	2	3.47	0.56	29	7.48	—	—	—	7.48	5.7	127.7	61.5	165.3	8.5	7.7	1.8	39	345	29	8	1	10	-64.853	-62.5274
bb180304-40	3	4.27	0.40	30	9.09	—	—	—	9.09	8.1	65.3	44.9	146.1	19.5	8.6	2.6	108	93	14	9	1	79	-64.8441	-62.861
bb180304-42	4	3.75	0.52	6	8.05	8.15	7.87	8.41	8.15	6.6	43.1	43.1	—	3.0	0.0	0.0	12	0	2	0	1	8	-64.857	-62.8583
bb180304-45	5	4.16	0.48	20	8.88	8.61	8.36	8.85	8.61	7.3	61.6	56.8	88.1	17.8	8.2	1.7	74	0	2	0	7	72	-64.8527	-62.8493
bb180305-42b	6	3.07	0.00	1	6.66	—	—	—	6.66	4.6	97.3	49.6	127.2	6.6	8.3	1.7	19	109	0	0	14	19	-64.8896	-62.8543
bb190224-48	7	2.57	0.30	10	5.63	5.85	5.47	6.21	5.85	3.6	31.2	31.2	—	1.1	0.0	0.0	5	0	0	4	0	5	-64.8133	-62.7129
bb190224-52	8	2.15	0.29	22	4.76	4.65	4.31	5.01	4.65	2.4	130.0	81.1	184.6	13.0	7.1	1.9	87	228	41	7	1	48	-64.794	-62.7098
bb190225-54	9	3.58	0.42	29	7.70	8.09	7.93	8.25	8.09	6.5	57.3	57.3	—	7.4	0.0	0.0	69	0	139	14	0	10	-64.8634	-62.5739
bb190225-55	10	4.24	0.50	20	9.04	8.86	8.73	9.00	8.86	7.7	63.3	63.3	—	7.5	0.0	0.0	39	0	158	13	0	13	-64.8589	-62.5774
bb190225-57	11	3.41	0.59	27	7.36	—	—	—	7.36	5.5	71.9	65.5	90.5	5.5	0.2	0.9	54	3	68	9	1	9	-64.8699	-62.5387
bb190226-48	12	2.91	0.47	30	6.33	—	—	—	6.33	4.2	77.0	58.2	179.0	15.3	7.4	1.9	98	108	9	1	0	93	-64.8617	-62.6301
bb190226-51	13	3.37	0.63	32	7.27	—	—	—	7.27	5.4	81.7	54.6	190.4	12.3	7.4	1.9	74	115	15	0	0	70	-64.8617	-62.6324
bb190226-53 & bb190304-18	14 & 23	—	—	—	—	6.60	6.47	6.74	6.60	4.5	93.9	42.9	178.5	27.6	14.7	3.7	60	216	20	8	31	52	-64.8608	-62.6173
bb190226-56 & bb190301-18	15 & 19	3.14	0.58	32	6.81	6.61	6.47	6.76	6.61	4.5	142.8	55.1	239.0	39.9	22.1	5.6	55	452	24	5	23	41	-64.8607	-62.6418
bb190228-18*	16	—	—	—	—	5.99	5.86	6.12	5.99	3.8	16.8	16.8	—	0.5	0.0	0.0	0	0	1	0	0	0	-64.8596	-62.4881
bb190228-52 & bb190302-53	17 & 22	—	—	—	—	8.51	8.40	8.62	8.51	7.2	86.1	61.4	114.8	40.4	22.1	5.6	32	131	2	3	8	32	-64.8556	-62.4969
bb190228-55b & bb190306-52	18 & 27	3.99	0.85	25	8.52	7.12	7.02	7.23	7.12	5.2	103.0	72.5	136.6	40.8	22.1	5.6	63	153	62	3	20	34	-64.8658	-62.4512
	27	3.40	0.46	22	7.34																		-64.8382	-62.5326
bb190302-48	20	3.87	0.49	30	8.30	8.71	8.48	8.94	8.71	7.5	52.6	52.6	—	3.1	0.0	0.0	15	0	1	5	6	15	-64.8654	-62.5646
bb190302-52	21	3.86	0.45	29	8.27	8.20	7.89	8.51	8.20	6.7	89.6	55.0	139.1	24.4	15.9	3.6	132	327	1	5	7	132	-64.8702	-62.5309
bb190304-45	24	2.14	0.23	7	4.74	—	—	—	4.74	2.4	48.5	47.6	106.0	9.3	0.1	0.9	35	0	0	0	25	35	-64.8662	-62.5486
bb190304-51	25	2.91	0.56	8	6.34	—	—	—	6.34	4.2	36.3	32.9	85.9	15.4	8.3	1.7	44	8	0	0	28	43	-64.8585	-62.5989
bb190304-57	26	2.87	0.42	24	6.24	—	—	—	6.24	4.1	30.0	30.1	—	11.2	0.0	0.0	40	0	0	0	27	41	-64.8557	-62.6314
bb190309-52	28	—	—	—	—	7.24	6.91	7.57	7.24	5.3	67.1	45.6	188.9	22.7	8.8	1.7	103	115	1	1	28	101	-64.9075	-62.9061

* with < 1 hr of total deployment time, this animal was excluded from analysis.

UAS = unoccupied aerial system, L_{UAS} = length measured from photogrammetry. Feeding rates for animals with repeat deployments are pooled together. Deployments 18&27 were the only deployments with repeat measurements of VGB_{est} on the same individual and both measurements are displayed. Mass was estimated from L using the OLS relationships in[36]. Day, night and twilight hours refer to total deployment hours, while λ_f is calculated only during feeding bouts (the proportion of day and night feeding for each whale are in Fig. S2). Deployment bb190228-18 was excluded from summary analyses because deployment length < 1 hr, giving a total of 28 total deployments on 24 unique animals. One deployment, bb190228-18, was excluded from further analysis due to short attachment duration.

nature portfolio

Corresponding author(s): David E Cade

Last updated by author(s): Dec 24, 2022

Reporting Summary

Nature Portfolio wishes to improve the reproducibility of the work that we publish. This form provides structure for consistency and transparency in reporting. For further information on Nature Portfolio policies, see our Editorial Policies and the Editorial Policy Checklist.

Statistics

For all statistical analyses, confirm that the following items are present in the figure legend, table legend, main text, or Methods section.

n/a	Confirmed	
☐	☒	The exact sample size (*n*) for each experimental group/condition, given as a discrete number and unit of measurement
☐	☒	A statement on whether measurements were taken from distinct samples or whether the same sample was measured repeatedly
☐	☒	The statistical test(s) used AND whether they are one- or two-sided *Only common tests should be described solely by name; describe more complex techniques in the Methods section.*
☐	☒	A description of all covariates tested
☐	☒	A description of any assumptions or corrections, such as tests of normality and adjustment for multiple comparisons
☐	☒	A full description of the statistical parameters including central tendency (e.g. means) or other basic estimates (e.g. regression coefficient) AND variation (e.g. standard deviation) or associated estimates of uncertainty (e.g. confidence intervals)
☐	☒	For null hypothesis testing, the test statistic (e.g. *F*, *t*, *r*) with confidence intervals, effect sizes, degrees of freedom and *P* value noted *Give P values as exact values whenever suitable.*
☒	☐	For Bayesian analysis, information on the choice of priors and Markov chain Monte Carlo settings
☒	☐	For hierarchical and complex designs, identification of the appropriate level for tests and full reporting of outcomes
☒	☐	Estimates of effect sizes (e.g. Cohen's *d*, Pearson's *r*), indicating how they were calculated

Our web collection on statistics for biologists contains articles on many of the points above.

Software and code

Policy information about availability of computer code

Data collection	No software was used to collect data in this study.
Data analysis	MATLAB code used for tag data processing and analysis has been released in Cade et al., 2021, Anim Biotelemetry, https://doi.org/10.1186/s40317-021-00256-w. MorphoMetriX, described in Torres and Bierlich, 2020 (https://joss.theoj.org/papers/10.21105/joss.01825.pdf) was used for analysis of photogrammetry data for determining animal length.

For manuscripts utilizing custom algorithms or software that are central to the research but not yet described in published literature, software must be made available to editors and reviewers. We strongly encourage code deposition in a community repository (e.g. GitHub). See the Nature Portfolio guidelines for submitting code & software for further information.

Data

Policy information about availability of data

All manuscripts must include a data availability statement. This statement should provide the following information, where applicable:

- Accession codes, unique identifiers, or web links for publicly available datasets
- A description of any restrictions on data availability
- For clinical datasets or third party data, please ensure that the statement adheres to our policy

The datasets analyzed during the current study are available at Stanford's digital repository, https://purl.stanford.edu/pm378wm1385. This deposit includes

processed bio-logging data describing animal orientation, motion and position; video data used to calculate engulfment timing; audited feeding data including indices of identified foraging events and start and end points of feeding bouts; summarized foraging data for all species; and UAV imagery and length analysis.

Human research participants

Policy information about studies involving human research participants and Sex and Gender in Research.

Reporting on sex and gender	No human research participants were used in this study
Population characteristics	No human research participants were used in this study
Recruitment	No human research participants were used in this study
Ethics oversight	No human research participants were used in this study

Note that full information on the approval of the study protocol must also be provided in the manuscript.

Field-specific reporting

Please select the one below that is the best fit for your research. If you are not sure, read the appropriate sections before making your selection.

☐ Life sciences ☐ Behavioural & social sciences ☒ Ecological, evolutionary & environmental sciences

For a reference copy of the document with all sections, see nature.com/documents/nr-reporting-summary-flat.pdf

Ecological, evolutionary & environmental sciences study design

All studies must disclose on these points even when the disclosure is negative.

Study description	Our study involved the collection of bio-logging data from Antarctic minke whales using suction-cup attached tags. Tag data were collected in concert with photogrametric measurements of whale length. Minke whale feeding rates during different diel periods and at different depths were compared to previously collected data from other species. Tag data was used to determine the temporal constraints on feeding.
Research sample	We tagged 28 whales, of which 24 were unique animals. 438 total hours of data were collected and processed. 18 animals had associated photogrametric length measurements, and length was determined for the other 6 animals from an allometric regression of length and an estimate of buccal cavity length.
Sampling strategy	Animals were sampled opportunistically. Bays were surveyed in small boats for whales and tags were attached whenever animals were found and when they were in behavior states amenable to approach by small boats
Data collection	Data was collected and processed by the authors.
Timing and spatial scale	Data was collected in February and March 2018 and 2019. All data was collected in Andvord Bay in the West Antarctic Peninsula or the adjoining Paradise Bay. The limited spatial and temporal scale allowed for relative stable environmental controls.
Data exclusions	Three additional minke whales had tags affixed for < thirty minutes so were excluded from analysis.
Reproducibility	All fieldwork, data processing, and analysis methods are given in high-level detail in the manuscript and allow for replication.
Randomization	In most cases, the entire data set was studied. In cases where individual lunge events were analyzed for kinematic parameters, 30 events for each individual were randomly chosen (using a random number generator in Matlab). Details in methods section.
Blinding	Analysis and summary of all data was conducted independently before hypotheses were tested so as not to bias results.

Did the study involve field work? ☒ Yes ☐ No

Field work, collection and transport

Field conditions	Fieldwork was only conducted on days when the weather permitted small boat operations; only days with minimal to moderate wind and swell.
Location	All data were collected in Andvord Bay in the West Antarctic Peninsula or the adjoining Paradise Bay.

Access & import/export	All work was conducted under National Marine Fisheries Services permits (#23095 and 16111), and Antarctic Conservation Act permits 2020-016, as well as institutional animal care protocols approved by the University of California, Santa Cruz
Disturbance	Suction-cup tagging and UAV photogrammetry are non-invasive research techniques, but do involve small boat approaches. All efforts were made to minimize disturbance from boat approaches, and tag records and video confirm that animals returned to normal behavior typically within 1 dive of tag attachment.

Reporting for specific materials, systems and methods

We require information from authors about some types of materials, experimental systems and methods used in many studies. Here, indicate whether each material, system or method listed is relevant to your study. If you are not sure if a list item applies to your research, read the appropriate section before selecting a response.

Materials & experimental systems

n/a	Involved in the study
☒	☐ Antibodies
☒	☐ Eukaryotic cell lines
☒	☐ Palaeontology and archaeology
☐	☒ Animals and other organisms
☒	☐ Clinical data
☒	☐ Dual use research of concern

Methods

n/a	Involved in the study
☒	☐ ChIP-seq
☒	☐ Flow cytometry
☒	☐ MRI-based neuroimaging

Animals and other research organisms

Policy information about studies involving animals; ARRIVE guidelines recommended for reporting animal research, and Sex and Gender in Research

Laboratory animals	n/a
Wild animals	All animals were studied in vivo after a minimally invasive procedure (attachment of a suction-cup tag) that does not involve restraint or capture and only involves approach of a wild animal by a small boat. All work was conducted under National Marine Fisheries Services permits (#23095 and 16111), and Antarctic Conservation Act permits 2020-016, as well as institutional animal care protocols approved by the University of California, Santa Cruz
Reporting on sex	sex was not reported in this study
Field-collected samples	not relevant for this study
Ethics oversight	Animal care protocols were approved by the University of California, Santa Cruz

Note that full information on the approval of the study protocol must also be provided in the manuscript.

nature ecology & evolution

Article

https://doi.org/10.1038/s41559-023-01993-2

Minke whale feeding rate limitations suggest constraints on the minimum body size for engulfment filtration feeding

In the format provided by the authors and unedited

Supplementary Information

Supplementary Box 1- Metabolic scaling exponent

There are reasonable debates as to the most appropriate metabolic scaling exponent, and the empirical work cited found scaling exponents ranging from 0.63 to 1 [95-104]. Although metabolic rate has never been explicitly measured in baleen whales, of the two most commonly cited exponents, 0.67 and 0.75, we use the higher one as both larger animals generally [102,103] and artiodactyls specifically [104] tend to have higher metabolic scaling exponents. Indeed, in order to account for mysticetes in the energy surplus model of Gearty et al.[30], an adjustment of the intake rate exponent from 0.71 to 0.78 was required. For our calculations, smaller intake rate scaling exponents would steepen the slope, implying minke whales would be further underperforming expectations, while larger intake rate scaling exponents would have the opposite implication.

Supplementary Box 2- Seasonal variation

Due to the temporal constraints on feeding, the negative scaling of feeding rates with body size at night combined with the neutral scaling during the day imply that the diel difference between nighttime and daytime feeding rates within foraging bouts was greater for small whales than for large whales (Fig 2i). Within AMW, daytime feeding rates for a 5 m AMW were 24% of the nighttime rates, while daytime feeding rates for a 9 m AMW were 41% of the nighttime rates. At the larger end of the rorqual whale size scale, a 22 m blue whale daytime feeding rate is 75% of the nighttime rate (Fig 2i). Under the assumption that the feeding rates and proportion of day and night feeding we observed would be maintained throughout the course of a nominal foraging season from Nov 1 to May 1, model results suggest that AMW feeding in our study area at the observed rates would not start performing more lunges at night than during the day until Feb 1 (Extended Data Fig 8b) and continue doing so for the remainder of the season.

From Nov 19 to Jan 24, when it never gets completely dark at our field site in the West Antarctic Peninsula (Extended Data Fig 8), if prey conditions, and, consequently, feeding rates, were the same as what we observed in late summer, our model suggests that whales > 7 m could account for the lost prime foraging time by foraging longer during the day, but smaller whales could not. As an extreme example, a whale of theoretically small size (3 m) would have to feed 42.5 hrs/day during the day to account for the lost ideal foraging time. Under alternative assumptions about the caloric value of lunges performed in surface-associated nighttime krill patches compared to daytime krill patches, that relationship changes somewhat (Extended Data Fig 8d). However, deep lunges would have to be 2.5 times as calorie-rich as shallow lunges in order for the theoretical 3 m whale to match its autumn intake rates by feeding 100% of its time. At that day:night calorie/lunge ratio, a 5 m whale would have to spend more than 22.7 hours per day feeding during the peak daylight time of year (Extended Data Fig 8d).

Supplementary Box 3- Strategies to overcome filter feeding minimum size constraints in neonates

A filter feeding minimum size constraint suggests two alternate strategies for juvenile forms of obligate filter-feeding species: 1) birth young at or above the minimum body size for suspension feeding, or 2) for some initial stage young must adopt an alternate feeding strategy, The limited data on neonate and juvenile members of filter feeding fish species seem to support these predictions. Manta and devil rays (*Mobula* sp.) and basking sharks (*Cetorhinus maximus*) give live birth to some of the largest neonates of all fish[105-108], which is likely to approximate the MSC of these species. Whale shark neonates, however, have been measured at less than 0.5 m[109], but have underdeveloped gill filtering structures[110] and filtering pads[111], and observations of younger individuals typically highlight more flexible foraging behavior, including suction feeding[112,113]. Little is known about the feeding habits of megamouth sharks (*Megachasma pelagios*); however, the only recorded individual caught by commercial longline was a juvenile specimen (190 cm total length), indicating that this individual was likely scavenging on particulate prey[114].

Supplementary Box 4- The effect of depth, density and seasonality on prey and feeding rate

As the density of krill within prey patches increases, rorqual whales increase their feeding rates to take advantage of high-quality food[48,90,91,115]. Given this trend, the 3-4 times greater feeding rates of AMW in shallow water (Fig 1b,c) are likely to indicate higher prey density per lunge, implying that the diel patterns we observe may underestimate the relative importance of nighttime feeding in relation to daytime feeding for small whales. Modeling results suggest that if prey behavior were to remain constant throughout the year (deep during the day, shallow at night), the extended day lengths in polar regions during the summer would be a critical environmental factor that limits engulfment filtration feeding at AMW body size. At the latitude of our study, if feeding rates and foraging durations were consistent throughout the year, total night lunges could exceed day lunges for 69% of the year (Extended Data Fig 8); however, for the majority of time AMW spend in the foraging region the sun is above the horizon – e.g. in our study area there is no true darkness from Nov 19 to Jan 24. If the observed feeding rates and diel proportions were maintained during midsummer, a 9 m whale would only perform 73% of the total lunges over 24 hrs we observed during the study period, while a 5 m whale would only perform 56% and a theoretical 3 m whale would only perform 44%.

Typical diel vertical migration patterns are often modified in polar summers, however. For instance, in a comparative seasonal study on West Antarctic Peninsula krill, summer krill in the 1993 season were found to be more abundant in near-surface waters than in the fall[116]. Recent video evidence has shown that small swarms of krill at the surface may still be dense[117], suggesting that while larger animals like humpback whales may have to use herding strategies like bubble net feeding to aggregate smaller groups[117,118], smaller animals like AMW may still be able to take advantage of small, dense patches. Because shallow feeding during our study period was tightly coupled with night feeding, our model of seasonal total feeding (Extended Data Fig 8) based on the proportion of night feeding could also be interpreted as a proportion of shallow feeding, demonstrating the greater dependence of shallow prey patches for smaller whales and supporting the suggestion that environmental conditions with surface-associated krill patches would be necessary to support small whales currently, and support their evolution in prehistoric oceans.

Other regions of the world also at times support productive surface patches of krill. In the Taranaki Bight, New Zealand, blue whales have been associated with krill patches that were densest in shallow (< 20 m) waters[119], and in the Gulf of St. Lawrence, Canada, blue whales feeding at night on shallow prey had feeding rates twice as high as during the day[91] coincident with shallow, dense prey patches [120]. These areas do not, however, currently support abundances of krill-feeding minke whales, suggesting that surface patches in these regions are not consistent enough to make engulfment filtration feeding worthwhile at small body sizes (Supplementary Box 5).

Supplementary Box 5- Temporal constraints on rorqual whale feeding

In rorqual whales, large body size minimizes the effects of the biomechanical, physiological and environmental constraints on feeding rate. Physiologically, increased oxygen stores coupled with lower mass-specific metabolic rate allow for longer and deeper dives in larger animals [35,121], increasing the time available for foraging at depth (Fig 4, Extended Data Fig. 5) or the oxygen available for metabolically expensive tasks like lunge feeding [35,53]. Biomechanically, increased engulfment capacity in larger animals allows for proportionally greater intake with every lunge, minimizing the overall number of lunges needed for a given intake. Accordingly, fewer lunges implies that the total time devoted to size-invariant constraints like approach and search time is decreased in larger animals. Conversely, smaller animals spend more total time searching for and approaching prey patches than do large ones.

Of the three phases of lunge feeding (acceleration, engulfment, and filtration), filtration time is the most dynamic, with the steepest relationship to body size (Fig 3) and the largest overall effect on lunge time. Due to the inflated buccal cavity and associated increased drag, the energetic cost of powered progress during filtration is high, so decreasing filter time increases the time available for other behaviors. Accordingly, small whales have relatively more baleen surface area which serves to decrease filter time [37,64,70]. However, as body size decreases, reductions in filter time have a proportionally lower effect on overall lunge time, leaving little scope to increase lunge rates by decreasing filter times (Extended Data Fig 6). The only way, then, for small animals like AMW to substantially increase their overall intake is to decrease the search time between lunges or to increase the amount of time actively foraging, both tactics limited by diurnal and seasonal temporal constraints as well as prey distribution patterns.

The amount of time available for foraging decreases with dive depth in AMW (Fig 4). Larger animals like blue whales, in contrast, can proportionally increase foraging time by decreasing surface time between dives, requiring only 32-51% of the time at the surface that an AMW does for a given dive length ([53], Extended Data Fig 5). When feeding near the surface, however, whales can combine breathing/recovery with the filtration and/or search phases (utilizing specialized oral plugs to keep water out of the gastrointestinal tract [122]), nearly removing the surface interval restriction as well as the transit time to depth, thereby allowing for ultra-high foraging rates in near-surface feeding (typically at night) (Fig 1b) that increase inversely with size (Fig 2g,j). The physiological constraints on dive duration relative to surface recovery time act more on smaller whales than larger whales (Fig 4), serving to limit the daytime (deep) feeding rates generally (Fig 2j), and explaining the observed lack of relationship between AMW daytime feeding rates and body length (Fig 5).

Supplementary References

105 Parker, H. W. & Stott, F. Age, size and vertebral calcification in the basking shark, *Cetorhinus maximus* (Gunnerus). *Zoologische mededelingen* **40**, 305-319 (1965).

106 Sund, O. Et brugdebarsel. *Naturen* **67**, 285-286 (1943).

107 Couturier, L. *et al.* Biology, ecology and conservation of the Mobulidae. *J. Fish Biol.* **80**, 1075-1119 (2012).

108 Broadhurst, M. K., Laglbauer, B. J. & Bennett, M. B. Gestation and size at parturition for Mobula kuhlii cf. eregoodootenkee. *Environ. Biol. Fishes* **102**, 1009-1014 (2019).

109 Aca, E. Q. & Schmidt, J. V. Revised size limit for viability in the wild: neonatal and young of the year whale sharks identified in the Philippines. *Asia Life Sciences* **20**, 361-367 (2011).
110 Garrick, J. Additional information on the morphology of an embryo whale shark. *Proceedings of the United States National Museum* **115**, 1-7 (1964).
111 Misty Paig-Tran, E. & Summers, A. Comparison of the structure and composition of the branchial filters in suspension feeding elasmobranchs. *The Anatomical Record* **297**, 701-715 (2014).
112 Boldrocchi, G. & Bettinetti, R. Whale shark foraging on baitfish off Djibouti. *Marine Biodiversity* **49**, 2013-2016 (2019).
113 Clark, E. & Nelson, D. R. Young whale sharks, Rhincodon typus, feeding on a copepod bloom near La Paz, Mexico. *Environ. Biol. Fishes* **50**, 63-73 (1997).
114 Amorim, A. F., Arfelli, C. A. & Castro, J. I. Description of a juvenile megamouth shark, Megachasma pelagios, caught off Brazil. *Environ. Biol. Fishes* **59**, 117-123 (2000).
115 Friedlaender, A. S. *et al.* The advantages of diving deep: Fin whales quadruple their energy intake when targeting deep krill patches. *Funct. Ecol.* **34**, 497-506 (2020).
116 Lascara, C. M., Hofmann, E. E., Ross, R. M. & Quetin, L. B. Seasonal variability in the distribution of Antarctic krill, Euphausia superba, west of the Antarctic Peninsula. *Deep Sea Research Part I: Oceanographic Research Papers* **46**, 951-984 (1999).
117 Cade, D. E., Kahane-Rapport, S. R., Wallis, B., Goldbogen, J. A. & Friedlaender, A. S. Evidence for size-selective predation by Antarctic humpback whales. *Frontiers in Marine Science* **9**, 747788, doi:https://doi.org/10.3389/fmars.2022.747788 (2022).
118 Acevedo, J., Plana, J., Aguayo-Lobo, A. & Pastene, L. A. Surface feeding behavior of humpback whales in the Magellan Strait. *Rev. Biol. Mar. Oceanogr.* **46**, 483-490 (2011).
119 Torres, L. G., Barlow, D. R., Chandler, T. E. & Burnett, J. D. Insight into the kinematics of blue whale surface foraging through drone observations and prey data. *PeerJ* **8**, e8906 (2020).
120 Guilpin, M. *et al.* Foraging energetics and prey density requirements of western North Atlantic blue whales in the Estuary and Gulf of St. Lawrence, Canada. *Mar. Ecol. Prog. Ser.* **625**, 205-223 (2019).
121 Halsey, L. G., Butler, P. J. & Blackburn, T. M. A phylogenetic analysis of the allometry of diving. *The American Naturalist* **167**, 276-287 (2006).
122 Gil, K. N., Vogl, A. W. & Shadwick, R. E. Anatomical mechanism for protecting the airway in the largest animals on earth. *Curr. Biol.* **32**, 1-6 (2022).